SANDIA REPORT
SAND2008-5112
Unlimited Release
Printed August 2008

Analytical Models for Total Dose Ionization Effects in MOS Devices

Philip M. Campbell and Carolyn W. Bogdan

Prepared by
Sandia National Laboratories
Albuquerque, New Mexico 87185 and Livermore, California 94550

Sandia is a multiprogram laboratory operated by Sandia Corporation,
a Lockheed Martin Company, for the United States Department of Energy's
National Nuclear Security Administration under Contract DE-AC04-94AL85000.

Issued by Sandia National Laboratories, operated for the United States Department of Energy by Sandia Corporation.

Available to DOE and DOE contractors from

U.S. Department of Energy
Officeof Scientific andTechnical Information
P.O. Box 62
Oak Ridge, TN 37831
Telephone: (865) 576-8401
Facsimile: (865) 576-5728
E-Mail: reports@adonis.osti.gov
Online ordering: http://www.doe.gov/bridge

SAND2008-5112
Unlimited Release
Printed August 2008

Analytical Models for Total Dose Ionization Effects in MOS Devices

Philip M. Campbell
Scientific Computing Systems

Carolyn W. Bogdan
Component Information and Models

Sandia National Laboratories
P.O. Box 5800
Albuquerque, NM 87185-1179

Abstract

MOS devices are susceptible to damage by ionizing radiation due to charge buildup in gate, field and SOI buried oxides. Under positive bias holes created in the gate oxide will transport to the Si / SiO_2 interface creating oxide-trapped charge. As a result of hole transport and trapping, hydrogen is liberated in the oxide which can create interface-trapped charge. The trapped charge will affect the threshold voltage and degrade the channel mobility. Neutralization of oxide-trapped charge by electron tunneling from the silicon and by thermal emission can take place over long periods of time. Neutralization of interface-trapped charge is not observed at room temperature. Analytical models are developed that account for the principal effects of total dose in MOS devices under different gate bias. The intent is to obtain closed-form solutions that can be used in circuit simulation. Expressions are derived for the aging effects of very low dose rate radiation over long time periods.

Acknowledgements

The authors are grateful to Jim Schwank for many helpful comments on an early version of this manuscript. Jim also provided to us a copy of his NSRE short course on total dose effects, reference [1], which is a comprehensive and most valuable document, clearly the place to start for anyone interested in the field. Thanks to Albert Nunez for providing measurements on power MOSFETs and to Eric Keiter for model implementation in Xyce.

Contents

Tables

Figures

This Page Intentionally Left Blank

1. Basic Mechanisms

When a gate oxide is exposed to ionizing radiation, electron-hole pairs are formed uniformly throughout the oxide. Electrons are extremely mobile and are quickly swept out of the oxide under the gate electric field. The holes that escape initial recombination drift toward one of the two interfaces, $gate/SiO_2$ or Si/SiO_2, depending on the sign of the applied field. Holes will be trapped in the strained region of the oxide near the interface creating a positive oxide-trapped charge. The trapping centers are neutral oxide defects (oxygen vacancies) that can trap holes and hold them for long periods. In radiation-hardened gate oxides the distribution of trapped holes is normally within a few nanometers of the interface. In field oxides and some commercial oxides trapped holes can be distributed throughout the bulk of the oxide.

As a result of the hole transport and trapping process, hydrogen (H^+) is released from hydrogen-containing defects in the oxide. The hydrogen will drift to the Si/SiO_2 interface where it can interact to form interface traps (dangling bonds in Si). For n-channel devices interface traps are negatively charged, and for p-channel devices interface traps are positively charged. Excellent summaries of total dose effects are given in references [1][2],

In what follows analytical models are developed that account for the dominant effects of total integrated dose and low dose aging in MOS devices. Two models are required, the bulk model and the zero-field model. The objective is to obtain analytical, closed-form solutions that can be applied to circuit simulation rather than building more comprehensive numerical models.

2. Threshold Voltage Shift

A positive oxide-trapped charge distribution introduces a negative threshold voltage shift given by [3]

$$\Delta V_{ot} = \frac{-1}{\varepsilon_{ox}} \int_0^{tox} \rho(x) x dx = -\frac{q}{\varepsilon_{ox}} \bar{x} \Delta N_{ot}, \qquad (1)$$

where x is distance from the gate electrode, $\varepsilon_{ox} = 3.45 \times 10^{-13}$ F/cm is the oxide permittivity, q is the electron charge, t_{ox} is the oxide thickness, ρ(x) is the distribution of trapped charge in $coul/cm^3$, ΔN_{ot} is the sheet density of trapped charge in cm^{-2}, and $\bar{x}$ is the centroid of the charge distribution which is assumed concentrated about $\bar{x}$. With a positive gate bias, the trapping sites are usually located within a few nanometers of the Si/SiO_2 interface. In this case $\bar{x} \cong t_{ox}$, and

$$\Delta V_{ot} = -\frac{q}{C_{ox}} \Delta N_{ot} \ ,$$

where $C_{ox} = \varepsilon_{ox} / t_{ox}$ is the oxide capacitance per unit area. With a negative gate bias where the holes are trapped near the $gate / SiO_2$ interface, $\bar{x} << t_{ox}$.

The voltage shift due to interface-trapped charge is given by

$$\Delta V_{it} = \frac{q \Delta N_{it}}{C_{ox}} dtype, \tag{2}$$

where q is the electron charge, ΔN_{it} is the sheet interface charge density in cm^{-2}, and dtype is +1 for n-channel devices and -1 for p-channel devices. The total threshold voltage shift is the sum of the two contributions,

$$\Delta V_{th} = \Delta V_{ot} + \Delta V_{it} \ . \tag{3}$$

The shift for holes trapped in the oxide is always negative, but the shift due to interface-trapped charge can be either positive or negative depending on the type of device.

3. Effect on Carrier Mobility

The presence of interface-trapped charge reduces inversion-layer carrier mobility. The mobility degradation can be expressed as [4] [5],

$$\mu = \frac{\mu_0}{1 + \alpha \Delta N_{it}} , \tag{4}$$

where μ_0 is the pre-radiation mobility and $\alpha \approx 1 \times 10^{-11}$ is a constant. The expression in Equation (4) may not be valid for short times after irradiation because of the presence of oxide-trapped charge close to the interface which would also affect mobility. At later times electron tunneling from the Si neutralizes oxide charge close to the interface, and only interface-trapped charge has an effect on mobility.

4. Electron-Hole Pair Generation, Recombination and Yield

The rate at which electron-hole pairs are injected into the oxide by radiation is given by

$$\frac{dN}{dt} = G_0 RY \ , \tag{5}$$

where G_0 is the generation rate, $8.1\times10^{12}\,cm^{-3}/rad$ in SiO_2, R is the dose rate in rads/sec and Y is the yield of e-h pairs. Charge yield varies because only a fraction of the holes formed will escape initial recombination. This fraction is dependent on the electric field as shown in Figure 1 [6]. The analysis in reference [6] is based on the observation that the hole trapping cross section is proportional to $E^{-0.55}$. An empirical fit to Figure 1 is given by $Y \cong 0.49\left[1+\tanh\left(1.2\log_{10}(E)\right)\right]$.

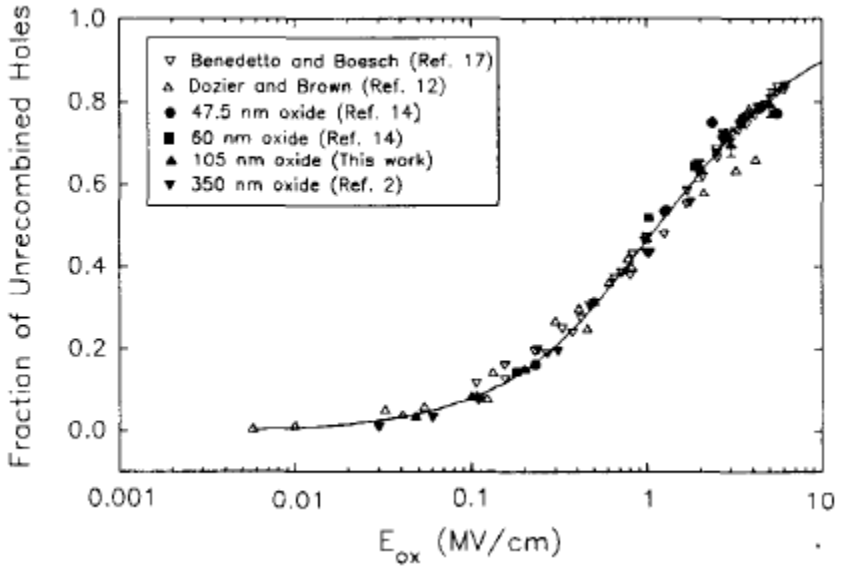

Figure 1 Fraction of Holes Generated by 10 KeV X-Rays that Survive Initial Recombination [6].

5. Hole Transport in the Gate Oxide

Although electrons move rapidly out of the oxide under the action of an applied field, holes have much lower mobility and a higher susceptibility to trapping. The number of trapped and transporting holes in the oxide of a MOS capacitor can be determined by measuring the flatband voltage shift. Experiments show that the transport of holes in the oxide is sensitive to both the electric field and temperature [7] [8]. The recovery of the flatband voltage shift takes place in milliseconds or less at room temperature with MV/cm fields. For low temperatures and very low fields, the holes are effectively frozen in place.

The transport of holes is by polaron hopping which is a phonon-assisted process. As a hole moves through the lattice it causes a distortion of the local potential field, increasing the trap depth and the probability of trapping at a local site. This transport process is

described by the biased continuous time random walk model, CTRW [9]. However, for most of the work presented here we assume holes generated in the oxide are quickly swept into the trapping region near the interface and transport effects are neglected. (Typical hole drift times are 10^{-7} sec.)

6. Rate Equation for Trapping of Holes

The density of trapped holes, p_t, in the strained region of the oxide near the Si/SiO_2 boundary is described by the rate equation [10][11],

$$\frac{dp_t}{dt} = (N_T - p_t)\sigma_T f_p - \frac{p_t}{\tau}, \tag{6}$$

where N_T is the density of trapping sites, $\sigma_T = \sigma_0 E^{-0.55}$ is the field-dependent cross section [6] for capture of a hole into a trap site, f_p is the flux of holes into the trapping region and τ is the characteristic time for trapped holes to recombine by electron tunneling from the silicon and by thermal emission of electrons from the oxide valence band. As discussed above we ignore transport effects and assume the holes appear immediately in the trapping region under the action of the gate bias. With this assumption the flux can be written, $f_p = G_0 YRt_{ox}$, where t_{ox} is the oxide thickness. For the moment we ignore recombination and write the rate equation as

$$\frac{dp_t}{dt} + G_0 YR\sigma_T t_{ox} p_t = G_0 YR\sigma_T t_{ox} N_T,$$

which has the following solution for the total density of oxide-trapped holes,

$$p_t = N_T\left[1 - \exp\left(-G_0 DY\sigma_T t_{ox}\right)\right], \tag{7}$$

where D is the total dose. The yield Y depends on the value of the oxide field as shown in Figure 1. The capture cross section may vary between soft and hard oxides, but for purposes of discussion we assume as representative values the cross sections measured in reference [12]. This work identified two traps with different capture cross sections: $\sigma_0 \cong 1.4\times10^{-13}\,cm^2$ and $\sigma_0 = 3\times10^{-14}\,cm^2$, where E is given in units of MV/cm. A value of $\sigma_0 = 6\times10^{-14}\,cm^2$ was measured in reference [13].

It is generally found that little trapping of electrons occurs in the bulk of the oxide. However, there seem to be significant numbers of electrons trapped at large cross-section sites associated with trapped holes near the Si/SiO_2 interface. The hole traps, which are positively charged after hole capture, become efficient electron traps with electron capture cross sections of $\sigma_{Te} \approx 3\times10^{-13}\,cm^2$ [13]. The trapped electron forms a dipole rather than directly recombining with the hole.

The density of these trapped electrons is proportional to trapped hole density over a wide range of irradiation conditions [14]. It is found that for dry-gate oxides the number of trapped electrons is $0.48 \pm 9\%$ of the number of trapped holes, and for wet-gate oxides the ratio is $0.16 \pm 6\%$. Based on these measurements we can assume that the density of uncompensated trapped holes is $(1 - f_e) p_t$ where p_t is given by Equation (7) and $f_e = const.$ The sheet density of oxide-trapped charge, adjusted for trapped electron compensation, can then be written,

$$\Delta N_{ot} = N_T^{'} (1 - f_e)[1 - \exp(-G_0 DY \sigma_T t_{ox})], \tag{8}$$

where $N_T^{'}$ is the density of trapping centers in cm^{-2}. Equation (8) describes the buildup of trapped charge that originates in the bulk of the oxide under an applied bias and is an element of what we refer to as the bulk model.

7. Interface-Trap Formation

Holes created by radiation in the bulk of the oxide are swept to the interface under an externally-applied gate bias. During transport, holes interact with hydrogen-containing defects to produce H^+. Under a positive bias the H^+ drifts to the Si/SiO_2 interface where it reacts with Si-H trap precursors to produce Si dangling bonds (interface traps) . This two-stage model of interface trap buildup is called the hole trapping/hydrogen transport model $(HT)^2$ [15]. Experiments have shown that under positive bias nearly all the H^+ produced in the oxide is eventually converted to interface traps [16] [17] [18].

H^+ is released either in the bulk of the oxide or near the silicon interface. In dry gate oxides the time dependence of interface trap buildup under a positive bias appears to be essentially independent of oxide thickness indicating most of the H^+ originates from holes trapped near the Si/SiO_2 interface, a result confirmed independently in reference [14]. On the other hand for wet gate oxides, there appears to be a significant amount of H^+ produced in the bulk of the oxide [15]. It is apparent that the way hydrogen is incorporated in the oxide during processing can affect where hole trapping and H^+ production will occur, the time for interface trap buildup, and the dependence on oxide thickness.

Studies with post-irradiation exposure to a hydrogen ambient [16] indicate the reactions responsible for H^+ production from hydrogen-containing defects during hole transport and trapping are:

$$h^+ + DH \rightarrow H_0 + D^+$$
$$H_0 + H_0 \rightarrow H_2 \qquad (9)$$
$$H_2 + D^+ \rightarrow DH + H^+$$

where h^+ represents a hole, and DH is the hydrogen-containing defect . Density functional theory suggests that interface traps are created by the direct interaction of protons at the Si/SiO_2 interface by the reaction,

$$H^+ + H - Si \equiv Si \rightarrow H_2 + \bullet Si^+ \equiv Si \ , \qquad (10)$$

where $\bullet Si^+ \equiv Si$ indicates a positively charged silicon ion with a dangling bond back bonded to three silicon atoms [18] [19].

As holes drift through the oxide and interact with defects, according to Eqn. (9) one hydrogen-containing defect DH is converted to D^+ for every H^+ produced. The equation that describes this process is

$$\frac{\partial H^+}{\partial t} + \frac{\partial f_H}{\partial x} = (N_D - H^+)\sigma_H G_0 YRt_{ox}, \qquad (11)$$

where N_D is the density of hydrogen-containing defects DH, σ_H is the cross section for H^+ formation by holes, $G_0 YRt_{ox}$ is the rate at which holes are generated by radiation, and f_H is the flux of H^+ in the oxide.

If one assumes that H^+ transport effects are small during the time H^+ builds up in the oxide, one can neglect the flux gradient term. Eqn. (11) can then be written,

$$\frac{dH^+}{dt} + \sigma_H G_0 YRt_{ox} H^+ = N_D \sigma_H G_0 YRt_{ox}, \qquad (12)$$

which has the following solution for the total density of H^+ released in the oxide by hole transport and trapping,

$$H^+ = N_D\left[1 - \exp(-G_0 DY\sigma_H t_{ox})\right]. \qquad (13)$$

The time for buildup of interface-trapped charge according to the reaction in Equation (10) takes place over fairly long times ($\approx 10^4$ sec) and is dependent on oxide thickness and applied field [20]. The transport of H^+ is well represented by the CTRW model and is the rate-limiting step in interface charge buildup. The CTRW model cannot be described in terms of a simple formula, but for the moment we assume that proton

transport can be represented by an effective mobility μ_H. In that case the flux of H^+ can be written $f_H = H^+ \mu_H E$, where μ_H must be derived from CTRW.

As observed earlier, we will assume that all the hydrogen released in the oxide eventually finds its way into interface traps. Under this assumption, the rate equation is written,

$$\frac{d\Delta N_{it}}{dt} = N'_{SiH}\sigma_{it}\left(H_0^+ - \Delta N_{it}/t_{ox}\right)\mu_H E, \tag{14}$$

where σ_{it} is the cross section for capture of a proton to form an interface trap, and H_0^+ is the total density of protons released in the oxide from Equation (13). In Equation (14) the flux of protons available for trapping has been reduced by the number of protons already trapped. Assuming μ_H is constant, the solution of Equation (14) is

$$\Delta N_{it} = H_0 t_{ox}\left[1-\exp\left(-N'_{SiH}\sigma_{it}\frac{\mu_H E}{t_{ox}}t\right)\right]. \tag{15}$$

As $t \to \infty$, $\Delta N_{it} \to H'_0$, where the sheet density of protons formed in the oxide is found from Equation (13):

$$\Delta N_{it} \to H'_0 = N'_D\left[1-\exp\left(-G_0 DY\sigma_H t_{ox}\right)\right]. \tag{16}$$

Equations (8) and (16) together with Figure 1 describe the process whereby charge created in the bulk of the oxide under an applied gate bias forms oxide- and interface-trapped charge. We refer to this process as the bulk model in contrast to the zero-field model which describes the situation where there is no applied bias.

8. Neutralization of Trapped Charge

Measurements of the threshold voltage shifts, ΔV_{it} and ΔV_{ot}, at different dose rates over long periods (10^7 seconds) are presented in reference [21]. These measurements show that interface-trapped charge builds up over a relatively long period of time, $\approx 10^4$ seconds, in agreement with results of reference [20], but neutralization of interface-trapped charge is not observed.

In Figure 2 (Figure 1 in reference [21]) the neutralization of oxide-trapped charge is shown during anneal at room temperature for 60 nm oxides irradiated to 100 Krad at different dose rates. The devices were NMOS biased at +6V. It is clear from Figure 2 that oxide charge neutralization is linear in log(t) and dose-rate independent.

Annealing of charge trapped in the oxide near the silicon interface is found to be dependent on both bias and temperature. This dependence can be explained by two

mechanisms: (1) the tunneling of electrons from the silicon into oxide traps, and (2) the thermal emission of electrons from the oxide valence band into oxide traps [22].

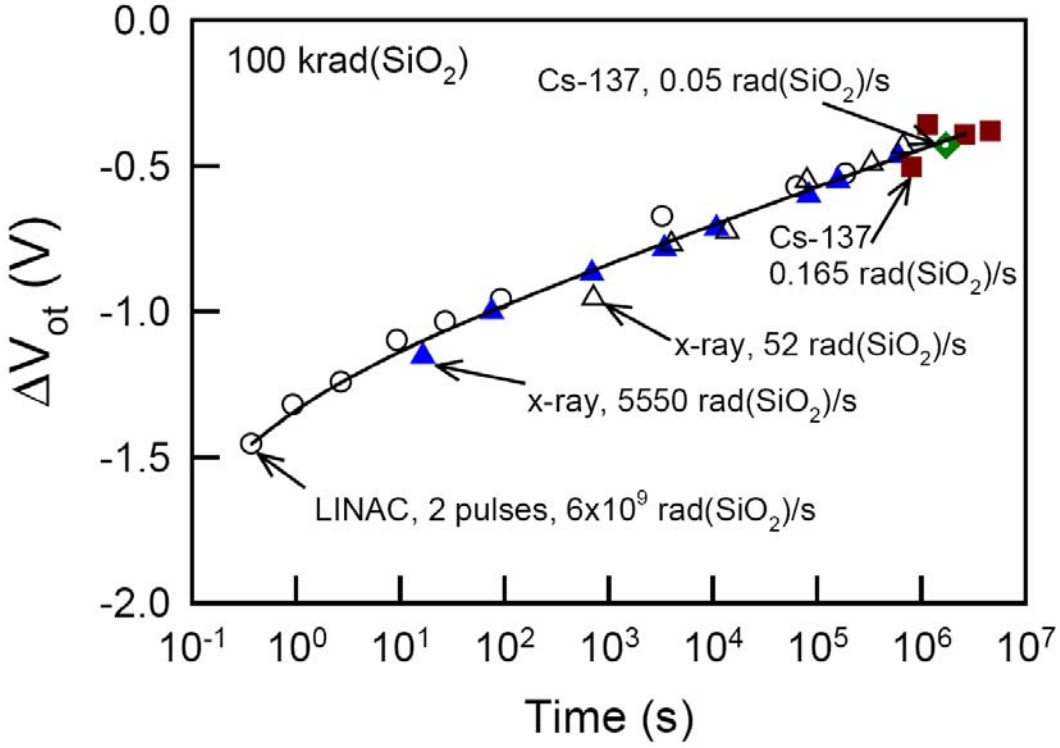

Figure 2 Annealing Curves for 100 Krad Total Dose and Different Dose Rates

From Figure 2 it is seen that the charge trapped in the oxide at time 2×10^{6} seconds is the same whether it was introduced nearly instantaneously by the LINAC or over the entire period at 0.05 rad/sec. This behavior is consistent with an electron tunneling front moving into the trapped charge near the interface. At low dose rate, holes move into the trapping region near the interface and build up ahead of the front to the same density that was created instantly with the LINAC. With a low dose rate trapped holes are neutralized as fast as they form behind the front.

The tunneling process can be understood as quantum mechanical penetration of free electrons into the potential barrier at the Si/SiO_2 interface [23]. This barrier, which is the difference in energy between the conduction bands of the oxide and of Si, is about 3.1 eV for electrons. Once into the barrier there is a certain probability of an electron being captured at a site with a trapped hole. The cross section for capture as viewed by an electron at the interface decreases exponentially with distance into the oxide [24]. This process leads to a tunneling front moving at a rate of 0.2 to 0.4 nm per decade in time. For a trap to be neutralized by tunneling it must be within about 4 nm from the interface.

Similarly, neutralization by thermal emission can be seen as a thermal emission front penetrating the bandgap of the oxide beginning close to the valence band and progressing towards the conduction band at a rate proportional to log(t). The thermal emission process varies exponentially with temperature but is independent of the spatial position of the trap. Although the thermal emission model predicts a strong temperature dependence it does not account for the bias dependence of the neutralization of hole traps. Since the tunneling model does predict the electric field dependence, it is evident that the annealing process is a combination of both mechanisms.

In reference [22] a combined tunneling and thermal emission model is described where the distribution of trapped holes $p_t(x,\phi_t,t)$ as a function of position, energy and time can be written

$$p_t(x,\phi_t,t) = p_0(x,\phi_t)e^{-(p_{tun}+p_{em})t}. \qquad (17)$$

In Equation (17), p_{tun} is the probability (rate) of electron tunneling out of the silicon into a trap, p_{em} is the probability (rate) of electrons being emitted out of the valence band into a trap, and $p_0(x,\phi_t)$ is the initial density of trapped holes in energy and position immediately following the radiation pulse. The rates are given by

$$p_{tun} = \alpha \exp(-\beta x) \quad \text{and} \quad p_{em} = AT^2 \exp(-\phi_t q / kT)\ , \qquad (18)$$

where $\alpha, \beta,$ and A are adjustable parameters, and ϕ_t is the energy difference between the trap and the valence band. The parameter β is related to the barrier potential, and α is the flux of free electrons at the Si interface times the capture cross section, σ_n.

In order to reproduce the annealing curve in Figure 2, consider the recombination rate due to tunneling given in Equation (18). The rate of charge loss in the oxide after the radiation pulse is over is

$$\frac{\partial p_t(x,t)}{\partial t} = -\alpha \exp(-\beta x) p_t\ ,$$

which has the solution

$$p_t(x,t) = p_0(x)\exp(-\alpha \exp(-\beta x)t)\ , \qquad (19)$$

where $p_0(x)$ is the spatial distribution of charge immediately after the radiation pulse.

This expression describes a tunneling front moving into the oxide from the Si/SiO_2 interface. Differentiating Equation (19) with respect to x, setting the derivative to zero and solving for x gives the position of the tunneling front as a function of time [22],

$$x_m(t) = \frac{1}{\beta}\ln(\alpha t)\ . \tag{20}$$

The expression for the tunneling front can be used along with Equation (1) to reproduce the annealing curve in Figure 2. First assume the oxide charge is uniformly distributed with density p_0 within a small distance x_0 of the silicon interface. Next rewrite Equation (1) so that x measures distance into the oxide from the interface and, assuming the charge density is zero behind the tunneling front, we have

$$\Delta V_{ot} = -\frac{qp_0}{\varepsilon_{ox}}\int_{x_m(t)}^{x_0}(t_{ox}-x)dx = -\Delta N_{ot}\frac{q}{C_{ox}}\left[\left(1-\frac{x_m}{x_0}\right)-\frac{x_0}{2t_{ox}}\left(1-\frac{x_m^2}{x_0^2}\right)\right].$$

In cases where $x_0 << 2t_{ox}$ the second term in square brackets can be dropped to give,

$$\Delta V_{ot} \cong -\Delta V_{ot}(0)\left[1-\frac{x_m(t)}{x_0}\right] = -\Delta V_{ot}(0)\left[1-\frac{1}{\beta x_0}\ln(\alpha t)\right]\ . \tag{21}$$

The initial point on the annealing curve, $\Delta V_{ot}(0)$, is where the tunneling front begins propagating at time $t = 1/\alpha$. The curve in Figure 2 is described by $\alpha = 8.44$ with $\beta x_0 = 24.8$ and $\Delta V_{ot}(0) = -1.4$. Figure 4 in reference [21] shows similar annealing curves for a total dose of 500 Krad on oxides 32 nm thick. Equation (21) reproduces these measurements with $\Delta V_{ot}(0) = -1.15$, $\alpha = 1.0$, and $\beta x_0 = 21.3$. As discussed in Section 6, the initial value of oxide charge density for a particular annealing curve, ΔN_{ot}, can be found from Equation (8).

A quantum mechanical analysis of the barrier penetration is given in reference [24]. This analysis gives for the parameters α and β,

$$\alpha = n_s\bar{v}\sigma_n, \qquad \beta = 2\kappa_0 = \frac{2}{\hbar}\sqrt{2m^*(W-E_e)}\ , \tag{22}$$

where n_s is the concentration of electrons at the semiconductor surface, $\bar{v}$ is the velocity of an electron, σ_n is the cross section for capture of an electron at a trapping site, W is the barrier height (surface potential), and E_e is the energy of an electron at the barrier. The barrier height is 3.1 eV, but corrected for image-force-induced barrier lowering [3] by a 1 MV/cm oxide field, the barrier becomes W=2.91 eV. We take a value for the effective mass, $m^* = 0.2m_0$, and $\bar{v} \approx 10^7$ cm/sec. The cross section σ_n is more uncertain, but we will adopt the value used in reference [24], $\sigma_n = 3\times10^{-15}$. Rewriting the expression for β gives,

$$\beta = \frac{2}{\hbar}\sqrt{2m^{*}W}\sqrt{1-\frac{E_e}{W}} = \beta_0\sqrt{1-\frac{qE_{ox}x_0}{W}}\,, \tag{23}$$

where $E_e = qE_{ox}x_0$ is the energy gained by the penetrating electron in the oxide field.

In the case of the parameters appropriate to Figure 2, where $\beta x_0 = 24.8$, Equation (23) gives $\beta = 6.5\times10^{7}$, which implies $x_0 = 3.8$ nm or 38 angstroms. This is a reasonable value, comparing closely with the work in reference [25] which found that the hole traps were within 3 to 4 nm from the interface and in reference [13] where 90% of the trapped charge was within 50 angstroms of the interface.

Deviations from simple log(t) annealing have been observed [25]. These deviations can be caused by a nonlinear spatial distribution of trapped holes or by a crossover from tunneling- to thermal emission-dominated annealing. The room-temperature curve in Figure 2 departs from the linear expression for times earlier than 10^2 sec. This is likely due to thermal emission which is considered next.

If we adopt the recombination rate due to thermal emission given in Equation (18), the rate of charge loss in the oxide after the radiation pulse is [22]

$$\frac{\partial p_t(x,\phi_t,t)}{\partial t} = -AT^2\exp(-\phi_t q/kT)p_t\,,$$

which has the solution

$$p_t(x,\phi_t,t) = p_0(x,\phi_t)\exp\left(-AT^2\exp(-\phi_t q/kT)t\right)\,, \tag{24}$$

where $p_0(x,\phi_t)$ is the distribution in position x and energy ϕ_t above the valence band of the oxide for trapped holes immediately after the radiation pulse. To make further progress analytically, we assume the x and ϕ_t variables are separable, i.e. $p_0 = p_1(x)p_2(\phi_t)$. This assumption just means the energy distribution of trapped holes is not position dependent.

Following the work in reference [22] it can be shown that Equation (24) represents a tunneling front for traps distributed in energy:

$$\phi_m(t) = \frac{kT}{q}\ln(AT^2t)\,. \tag{25}$$

Combining the tunneling front in energy with electron tunneling in position gives for the threshold voltage shift,

$$\Delta V_{ot} = -\frac{q}{\varepsilon_{ox}} \int_{\phi_m(t)}^{\phi_c} p_2(\phi_t) d\phi_t \int_{x_m(t)}^{x_0} (t_{ox} - x) p_1(x) dx \,, \tag{26}$$

where the tunneling fronts in position and energy are given by Equations (20) and (25).

In order to apply Equation (26) to the case of Figure 2, we assume p_1 is uniform within x_0, and p_1 and p_2 are normalized so the integral over p_2 is unity:

$$\Delta V_{ot} = -\Delta V_{ot}(0) \int_{\phi_m(t)}^{\phi_c} p_2(\phi_t) d\phi_t \left[\left(1 - \frac{x_m}{x_0} \right) - \frac{x_0}{2t_{ox}} \left(1 - \frac{x_m^2}{x_0^2} \right) \right]. \tag{27}$$

The distribution in energy will generally be complicated enough that Equation (27) will have to be handled numerically. A code that does this is given in the appendix. The distribution in energy shown in Figure 3 reproduces the departure from a straight line in log(t) in Figure 2 with T=300 ^{o}K and A=100. The energy distribution shown in Figure 3 is similar to an extraction given in reference [22], although the component centered at 0.55 eV above the valence band is relatively larger than that the smaller component in reference [22]. This twin-peak distribution is also seen in thermally-stimulated-current measurements, reference [14].

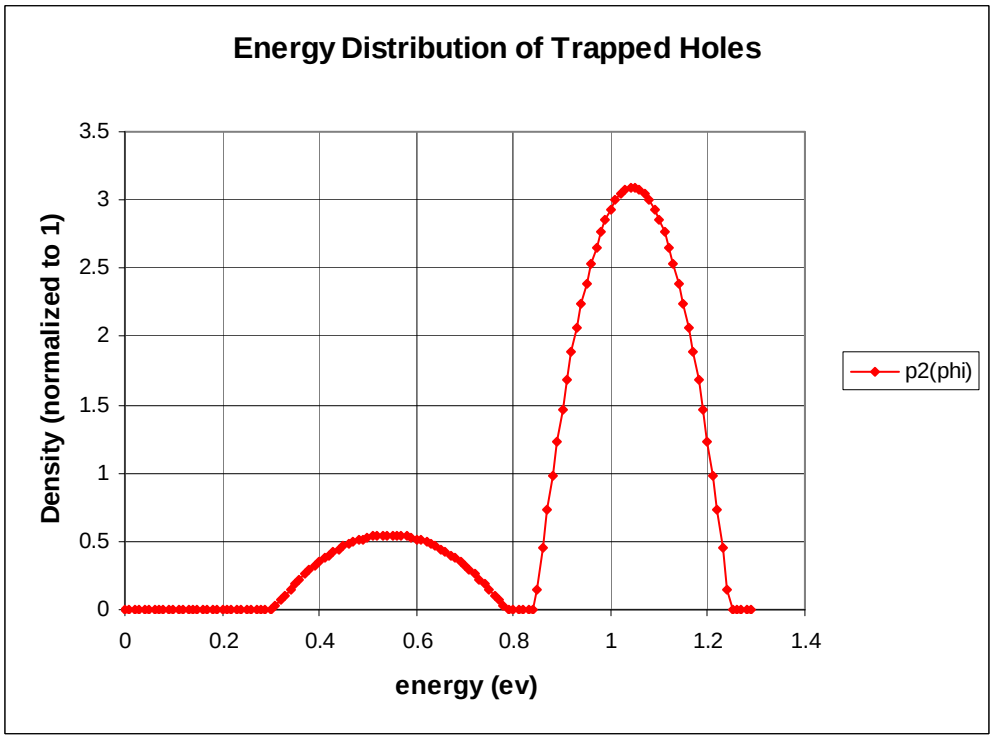

Figure 3 Energy Distribution of Trapped Holes Implicit in Figure 2.

9. Direct Measurement of Charge in Gate Oxides

In analyzing most published experimental results, what we will not know is the density and distribution of oxide trap sites and the density of hydrogen-containing defects in the oxide. Also, there may be different kinds of traps present with different cross sections. Values for these quantities will have to be derived from the data. Typical parameter values are given below in Tables 1 and 2.

In reference [21] n-channel CMOS devices were irradiated at various dose rates to 100 Krads, 230 Krads and 500 Krads. Threshold voltage shifts due to oxide charge and interface charge were measured. Assuming $\bar{x} \cong t_{ox}$, Equations (1) and (2) have been used to derive ΔN_{ot} and ΔN_{it} from measurements. The values are shown in Figure 4.

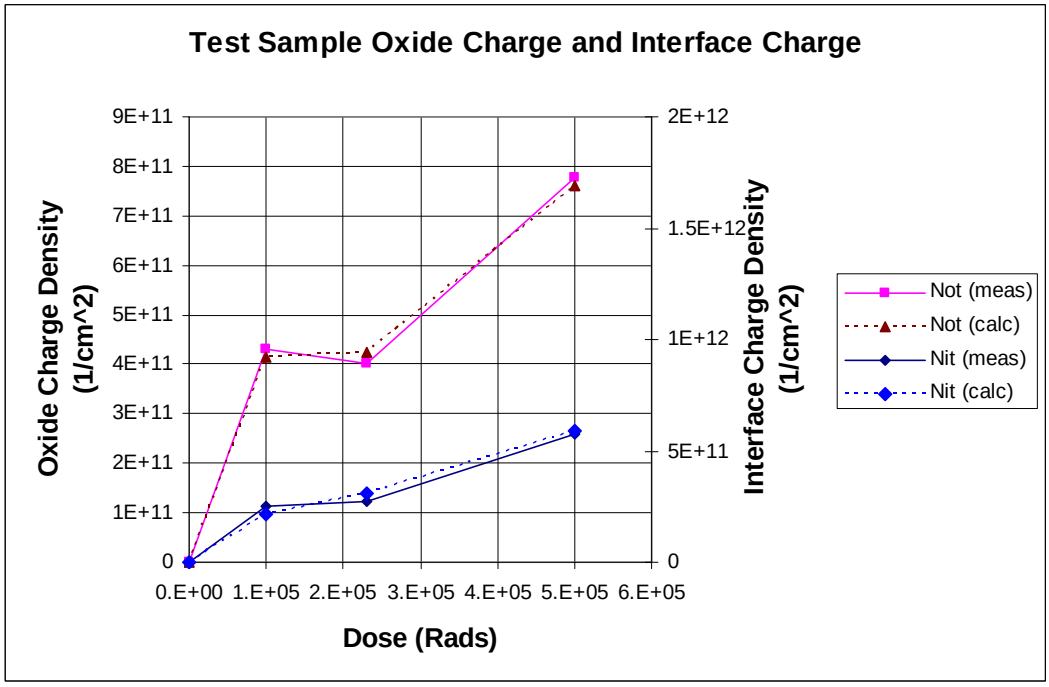

Figure 4 Oxide Charge and Interface Charge in MOS Test Samples Compared with Calculated Values.

The curves are not smooth in Figure 4 because the 100 Krad tests used an oxide thickness of $t_{ox} = 60$ nm and the other two tests used an oxide thickness of $t_{ox} = 32$ nm. The oxide charge measurements are matched well with Equation (8) using the higher value of capture cross section, $\sigma_0 = 1.4 \times 10^{-13} cm^2$ and a trap density of $N_T^{'} = 1.43 \times 10^{12} cm^{-2}$,

assuming $f_e << 1$. The interface charge density was calculated from Equation (16) using a cross section for H^+ formation of $\sigma_H = 6\times10^{-14}\,cm^2$ and a density of hydrogen-containing defects of $N_D^{'} = 1.59\times10^{12}\,cm^{-2}$. In all the tests the gate voltage was 6V with corresponding yield values of Y=0.5 for the 60 nm oxide and Y=0.6 for the 32 nm oxide.

In reference [14] a number of oxides were studied primarily to determine the electron trapping efficiency f_e that appears in Equation (8). In Table 1 below is summarized some of the results of reference [14] from the point of view of extracting parameters needed in Equations (8) and (16).

Table 1. Summary of Oxide Charge Measurements and Parameters for Analysis

Test	D	t_{ox}	$\Delta N_{ot}(meas)$	$\Delta N_{it}(meas)$	f_e	$N_T^{'}$	$N_D^{'}$
I	2×10^4	3.5×10^{-5}	1.21×10^{11}	2.2×10^{10}	0.19	1.56×10^{12}	1.04×10^{11}
II	1×10^6	4.7×10^{-6}	2.56×10^9	1.26×10^9	0.24	6.09×10^9	1.58×10^9
III	7×10^5	3.6×10^{-6}	2.00×10^9	1.00×10^9	0.31	7.88×10^9	1.73×10^9
IV	2×10^6	4.5×10^{-6}	2.1×10^{10}	5.2×10^9	0.55	3.25×10^{10}	5.45×10^9

The values for $N_T^{'}$ and $N_D^{'}$ were found assuming the trapping cross section is $\sigma_0 = 3\times10^{-14}$ and the cross section for hydrogen formation is $\sigma_H = 6\times10^{-14}$. In all these tests the gate oxide field was 2 MV/cm and Y=0.6.

The important information in Table 1 is the difference in the density of trapping sites and hydrogen-containing defects between the hard and soft oxides tested. Test I was done on a wet oxide with standard processing and the other tests were done on wet and dry oxides with special processing for hardness. In the hard oxides the density of trapping sites at the silicon interface is much smaller. The soft oxide in Test I has values much closer to the commercial oxides analyzed in the next section.

10. Measurement of Total Dose Effects in Commercial MOS Devices

A complex series of total dose measurements for n-channel MOSFETs IRF620 and IRF130 are available in the literature [26]. This reference describes a method of hardening whereby a MOSFET is pre-exposed to radiation and then annealed at 100 $°C$. This process leaves the device with trapped charge in the oxide which lowers the threshold voltage to a negative value. Circuits using the processed device are designed around the lower threshold voltage. The pre-exposure fills most of the oxide trap sites and also releases most of the H^+, which is later removed by annealing. The processed device is then less sensitive to subsequent radiation exposure.

Whatever the merits of this approach to hardening, the data reported in reference [26] provide a wealth of interesting tests for total dose models.

First consider the measured threshold voltage and mobility for the IRF620 irradiated with a gate bias of +10V. These values are shown in Fig. 5 as a function of dose. In Fig. 6 are shown oxide-trapped charge and interface-trapped charge derived from the data in Fig. 5 using Eqns. (1) - (4) with $\bar{x} = t_{ox}$ and $\alpha = 1 \times 10^{-11}$. We do not have construction analysis on the IRF620, but if we assume $t_{ox} = 120$ nm, $N_t^{'} = 8.0 \times 10^{12} cm^{-2}$ and $\sigma_0 = 6 \times 10^{-14} cm^2$, Equation (8) gives good agreement with the values derived from experiment as shown in Fig. 6.

Interface-trapped charge given by Equation (16) is shown in Fig. 6, with Y=0.4, $N_D^{'} = 6.9 \times 10^{11} cm^{-2}$ and $\sigma_H = 3 \times 10^{-14} cm^2$. The yield Y corresponds to a gate electric field during irradiation of 0.8 MV/cm.

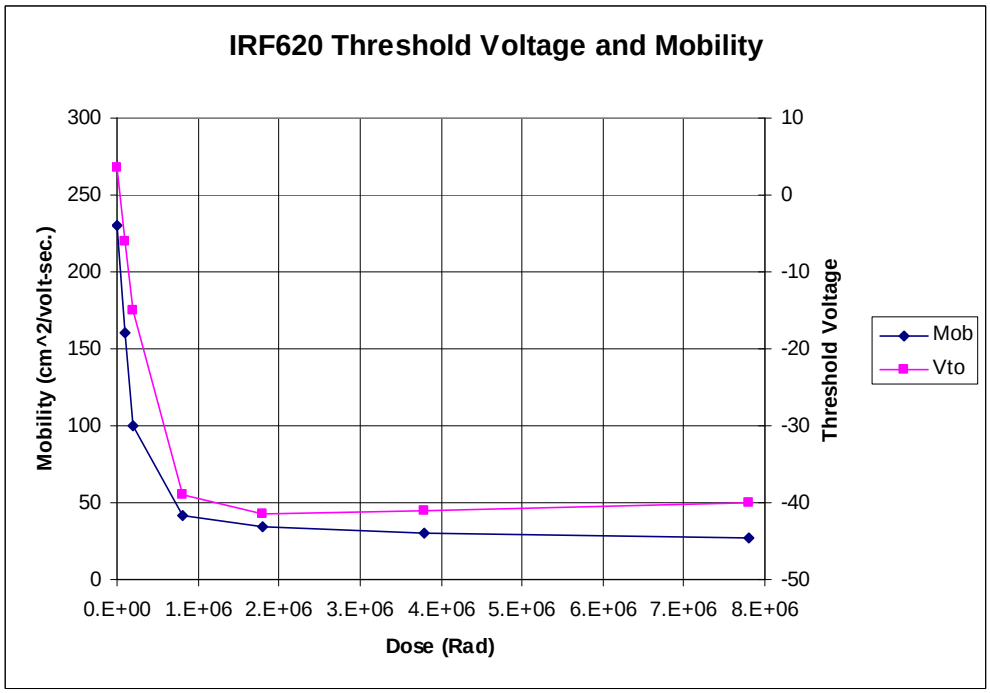

Figure 5 Measured Values of Threshold Voltage and Mobility for the IRF620.

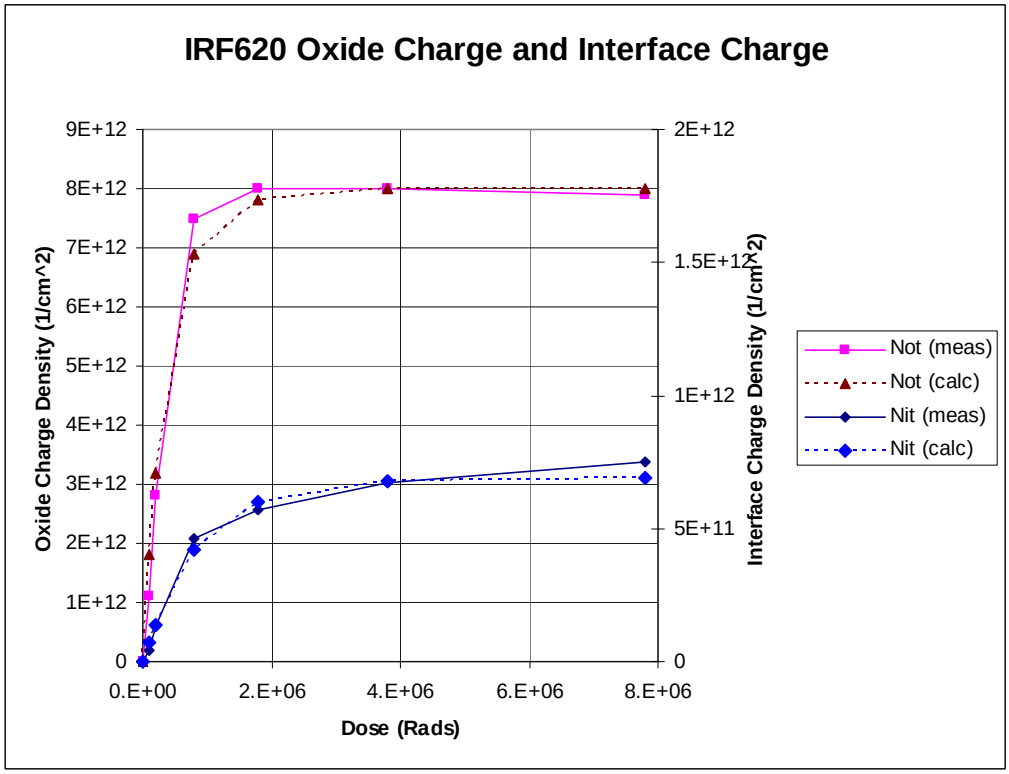

Figure 6 Measured and Calculated Values of Oxide-Trapped Charge and Interface-Trapped Charge for the IRF620 under Positive Gate Bias.

The bias dependence of radiation effects was an important issue in these studies. With positive bias the holes generated in the oxide by radiation are swept into the trapping region near the silicon boundary where a fraction of the holes are trapped. With negative gate bias, the holes are swept to the gate boundary where trapping also occurs. In the context of Equation (1), $\bar{x} \cong t_{ox}$ for positive bias, and $\bar{x} << t_{ox}$ for negative bias. So it is expected that the threshold shift for oxide-trapped charge will be much smaller for radiation under negative bias.

It is also possible to imagine a situation where the only trap sites are at the silicon interface and, with negative bias, only holes formed in the region of the traps will be captured. However, assuming the trap sites are near the gate interface gives a better match to the measurements shown here for the IRF620.

In analyzing the results for -10V bias in reference [26], we will assume the same amount of H^+ is generated by hole transport and trapping as in the case of +10V bias and, as long as the negative bias is not kept on too long, all the hydrogen released will find its way to the interface and be trapped there. After the negative gate bias is removed, the

hydrogen ions will diffuse over time into the trapping region at the silicon interface which can be thought of as a potential well for the capture of H^+.

Fig. 7 reproduces Figure 1 of reference [26] which shows the threshold shifts for the IRF620 at different gate bias. To extract from these curves the shift due to oxide charge, ΔV_{ot}, for the -10V case, we assume the same (positive) shift is present for interface charge, ΔV_{it}, that was derived for the case of positive gate bias and use Equation (3).

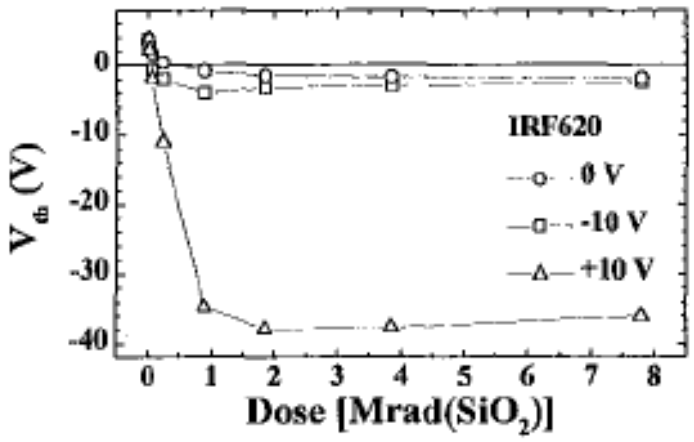

Figure 7. Measured Threshold Voltage Shifts for Different Gate Bias for the IRF620.

In the case of negative bias there are two unknowns, the sheet density of trapped charge, ΔN_{ot}, and the centroid of the charge distribution, $\bar{x}$. It is uncertain whether the type and density of trapping sites near the gate interface are similar to those near the silicon interface. The strain and distortion of the oxide lattice at the gate, which presumably results in trapping sites, may be different. There is no data that show unambiguously where the charge is trapped near the gate, but provisionally we will assume $\bar{x} = 0.2t_{ox}$, namely a distribution that is localized but still broader than the distribution of trapping centers near the silicon interface.

With these assumptions Equation (8) can be used with the same trapping cross section for the +10V case, $\sigma_0 = 6\times10^{-14}\,cm^2$, and a density of trapping sites of $N_t^{'} = 1.01\times10^{13}\,cm^{-2}$ to obtain a good match to the threshold shifts as shown in Figure 8. The trapped charge densities for the -10V case range from 2.0×10^{12} to 9.9×10^{12}, similar to the densities observed under positive bias. In Fig. 8 the threshold shifts back off at higher dose, because ΔV_{ot} saturates while ΔV_{it} (which is positive) does not.

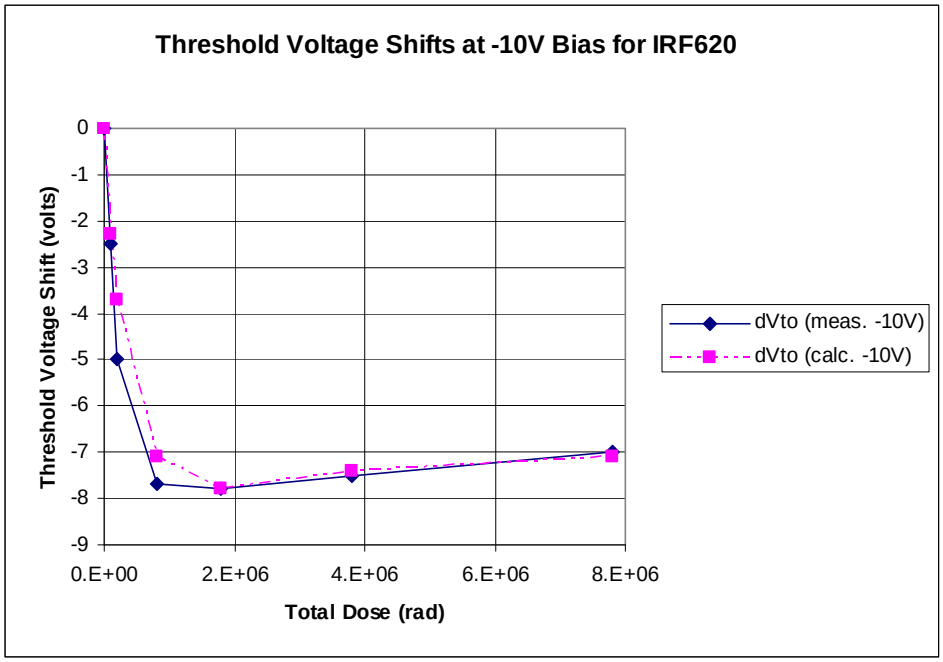

Fig. 8. Threshold Voltage Shifts for IRF620 at -10V Gate Bias

The situation with 0V bias has some essential differences from the -10V case even though the measured threshold shifts are of similar size. First, even with zero bias on the gate the field in the oxide is not strictly zero because of the work function difference between the gate material and the silicon, $\phi_{ms} = \phi_m - \phi_s$. In the present case $\phi_{ms} \cong -0.7$ volts [27] which has the same effect as a small positive field in the oxide equal to 0.06 MV/cm with $Y \approx 0.03$. (See Section 2.3.4.1 in reference [3].) These numbers, together with Equation (8), are too small to match the observed threshold shifts shown in Fig. 7.

Accordingly, we assume that with zero gate bias the charge yield in the bulk of the oxide is nearly zero. All the electron-hole pairs recombine before they can get away from each other. But at both boundaries of the oxide, the mobile electrons will see a sharp diffusion gradient and will diffuse out of the oxide leaving uncompensated holes to a depth δ. If we think of the sea of electron-hole pairs as a plasma, δ will correspond to the Debye length. In the interior of the oxide, nearly total recombination will occur as predicted in Fig. 1. In a thin layer at the boundaries, however, uncompensated holes will be captured in trap sites, and this trapped charge will cause a threshold voltage shift.

To calculate the width δ, first take as the space charge field in this region, $E = (q/\varepsilon_{ox})\Delta N$, which is that of a sheet distribution of charge where the density is $\Delta N = G_0 D\delta$. Electrons of temperature T can escape this region if the field is less than

$$E\delta = \frac{kT}{q} = \frac{q}{\varepsilon_{ox}} G_0 D\delta^2, \tag{28}$$

which gives for the depth of the charge distribution,

$$\delta = \sqrt{\frac{\varepsilon_{ox} kT}{q^2 G_0 D}}\,. \tag{29}$$

In order to derive expressions similar to Equations (8) and (16) for oxide-trapped charge and interface-trapped charge, it is assumed that the flux of holes into the trapping region is $f_p = G_0 R\delta$, similar to the derivation of Equation (7) except that the width of the region of uncompensated holes is δ instead of t_{ox}. From these considerations, the equations representing the zero-field model are,

$$\Delta N_{ot} = N_T^{'}[1-\exp(-G_0\sigma_T \delta D)], \tag{30}$$

$$\Delta N_{it} = N_D^{'}\left[1-\exp\left(-G_0\sigma_H \delta D\right)\right], \tag{31}$$

where we can assume σ_H is the same as used above, but $\sigma_T = \sigma_0 E^{-0.55}$ will require some adjustment. Since we are presumably in a low-field situation in the region δ, it is expected that $\sigma_T >> \sigma_0$, but the power law dependence of σ used above is probably not valid here. Intuitively, one would expect that most of the holes are instantly trapped after being formed with little residual motion in the region of the trapping sites. The H^+ will be formed in association with hole trapping right next to the interface.

Based on these considerations, we find that if $\sigma_T = 40\sigma_0$ and $N_T^{'} = 1.13\times10^{12}$, with $N_D^{'} = 6.9\times10^{11}$, the measured threshold voltage shifts for zero bias shown in Figure 7 can be reproduced with Equations (30) and (31) as shown in Figure 9. In Equations (30) and (31), $Y \cong 1$, because the lifetime for electron-hole recombination is greater than the time an electron spends in the region δ. The width of the region δ ranges from 2.19 nm at 100 Krad to 0.24 nm at 7.8 Krad, and the electron velocities are $\approx 10^7$ cm/sec.

Threshold voltage shifts are also measured for the IRF130 in reference [26], but since mobility measurements are not available for this device the interface-trapped charge can only be guessed at. However, an annealing curve is given for the IRF130 and is reproduced in Figure 10. The curve shown in Figure 10 is somewhat misleading because it is not plotted against log(t). Re-drawing the plot against log(t) reveals a perfectly straight line down to at least 100 hours. This curve is the electron tunneling curve and is matched by Equation (21) with $\Delta V_{ot}(0) = -14$, $\beta x_0 = 11.40$ and $\alpha = 0.1$, where time is

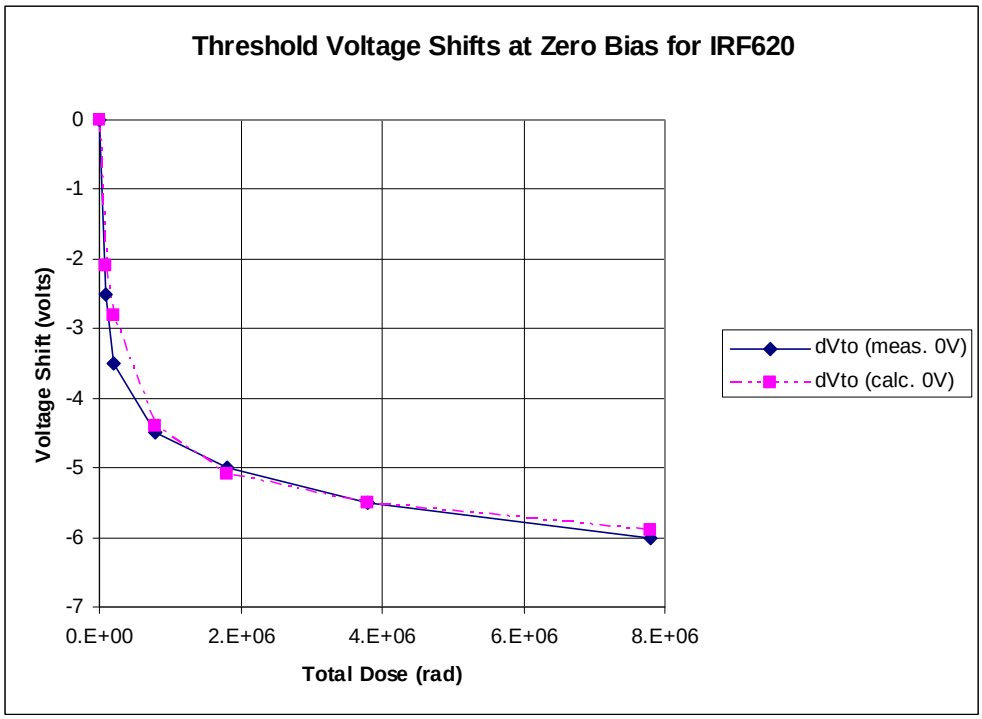

Fig. 9 Threshold Voltage Shifts for IRF620 at Zero Gate Bias

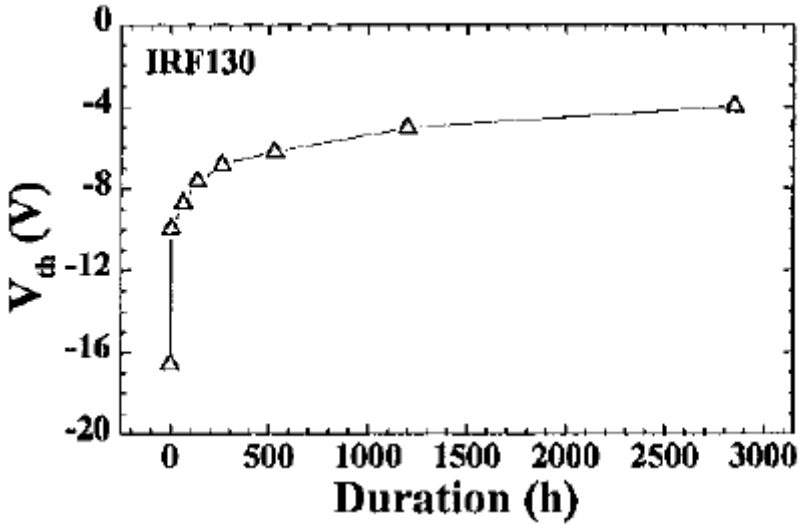

Fig. 10 Annealing Curve for the IRF130 at 100 *°C* after Irradiation at +15V.

measured in hours. These values together with Equation (23) yield a value for the size of the trapping region of $x_0 = 1.8\,\text{nm}$, comparable to the size of δ. The curve in Figure 10 begins after initial thermal emission has removed the low-lying states in energy and some of the interface-trapped charge.

That interface-trapped charge is greatly reduced by annealing at 100 $°C$ is evident in Figures 9 and 10 of reference [26], which show that after annealing the mobility is reduced by only 10% to 20% at high total dose. This mobility reduction corresponds to a value of interface-trapped charge of 1 or 2×10^{10} rather than 6 or 7×10^{11} that was present before annealing.

Measured I-V curves are available for the p-channel power MOSFET MTB30P06V for five total dose values from 20 Krad to 500 Krad, all obtained with a dose rate of 200 rad/sec [28]. The threshold voltage and mobility can be obtained from the I-V curves by parameter extraction. The results are shown in Fig. 11.

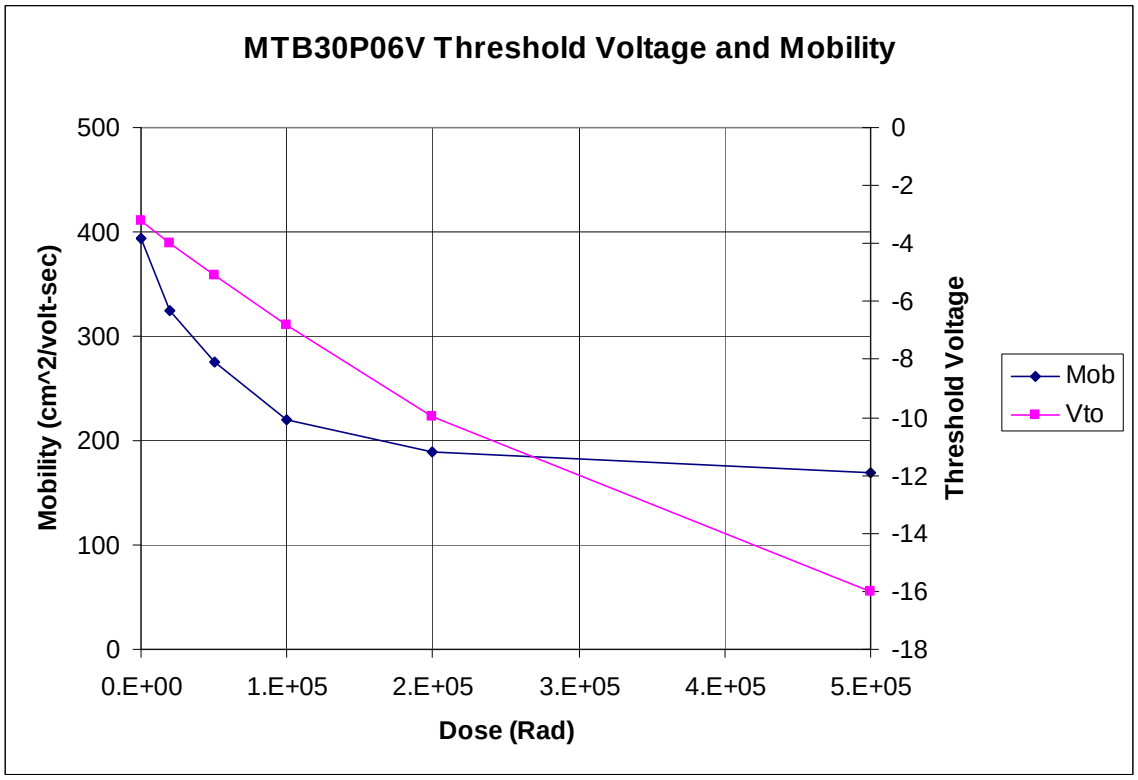

Figure 11 Threshold Voltage and Mobility as a Function of Total Dose for the MTB30P06V

From the data given in Fig. 11 it is possible to extract values for ΔN_{ox} and ΔN_{it} using Equations. (1) - (4). We don't have construction analysis for the MTB30P06V, but

parameter extraction indicates a value for the oxide thickness of $t_{ox} = 104.8$ nm. The value of gate bias during irradiation was -15V, giving an oxide field of E=1.4 MV/cm, and from Figure 1, Y=0.55. Since the gate bias during radiation was negative, we will assume $\bar{x} = 0.2t_{ox}$, the same value as indicated in the analysis of the IRF620. ΔN_{it} is first determined from the mobility values and then ΔN_{ot} is found from the threshold shifts using Equation (3). The values of oxide-trapped charge and interface-trapped charge derived from the measured values in Fig. 11 are shown in Fig. 12.

The oxide-trapped charge can be calculated from Equation. (8). With a density of trapping sites of $N_T' = 2.28\times10^{13}\ cm^{-2}$ and a cross section of $\sigma_0 = 6\times10^{-14}\,cm^2$, the calculated values of ΔN_{ot} from Equation. (8) are in agreement with values extracted from measurement as shown in Fig. 12 .

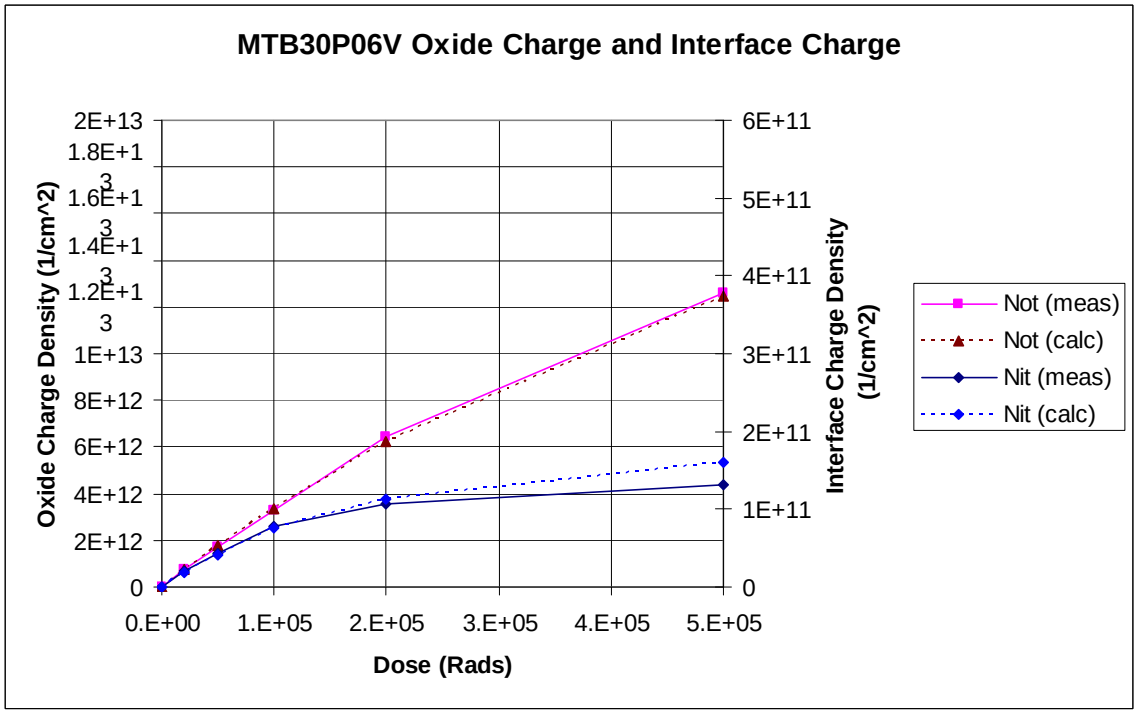

Figure 12 Measured and Calculated Values of Oxide-Trapped Charge and Interface-Trapped Charge for the MTB30P06V.

The interface-trapped charge can be calculated from Equation (16). We assume a value of $\sigma_H = 12\times10^{-14}\,cm^2$, and with Y=0.55, $N_D' = 1.7\times10^{11}\,cm^{-2}$, the calculated values match the data reasonably well as shown in Figure. 12.

Total dose measurements are also available for the p-channel power MOSFET NTB5605P [28]. Values of threshold voltage and mobility obtained by parameter extraction from I-V curves are shown in Fig. 13 for 108 Krad, 216 Krad and 328 Krad. Values of oxide-trapped charge and interface-trapped charge derived from the parameters extracted in Fig. 13 using Equations. (1) - (4) are shown in Fig. 14 along with calculated values from Equation. (8). The calculations used a value of t_{ox} = 107 nm. The gate bias was -10V with an oxide field of E=1.0 MV/cm, a trapping cross section of $\sigma_o = 1.4\times10^{-13}\,cm^2$, and a density of trapping sites $N_T^{'} = 1.19\times10^{12}\,cm^{-2}$. These calculations also assumed a centroid for the oxide-trapped charge of $\bar{x} = 0.2t_{ox}$. Interface-trapped charge is calculated from Equation (16) assuming $N_D^{'} = 5.0\times10^{10}\,cm^{-2}$ and $\sigma_H = 1.2\times10^{-13}\,cm^2$. Calculated values of ΔN_{it} are shown in Fig 14.

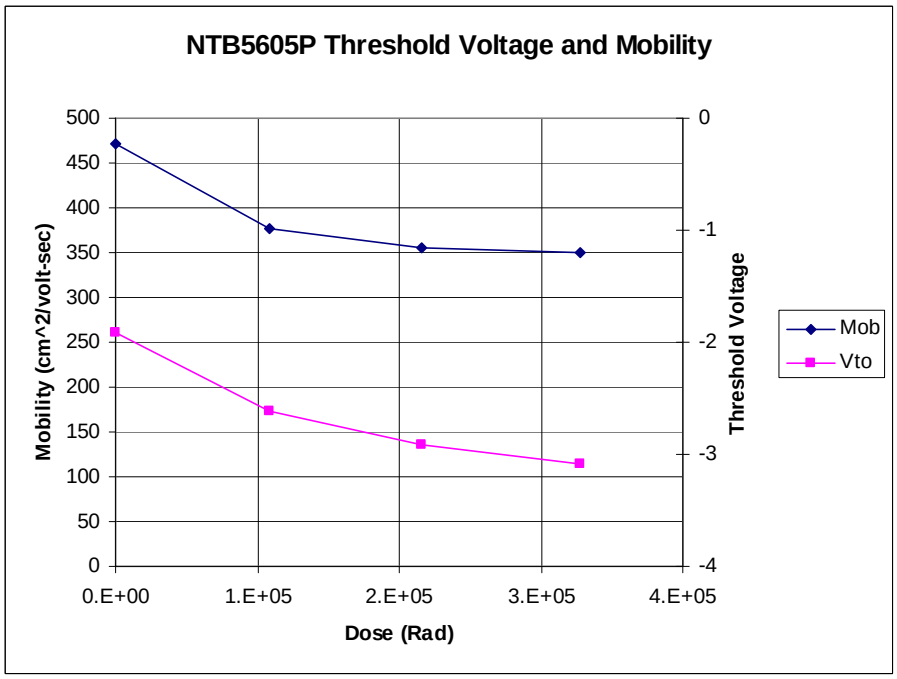

Figure 13 Threshold Voltage and Mobility Extracted from I-V Curves for NTB5605P

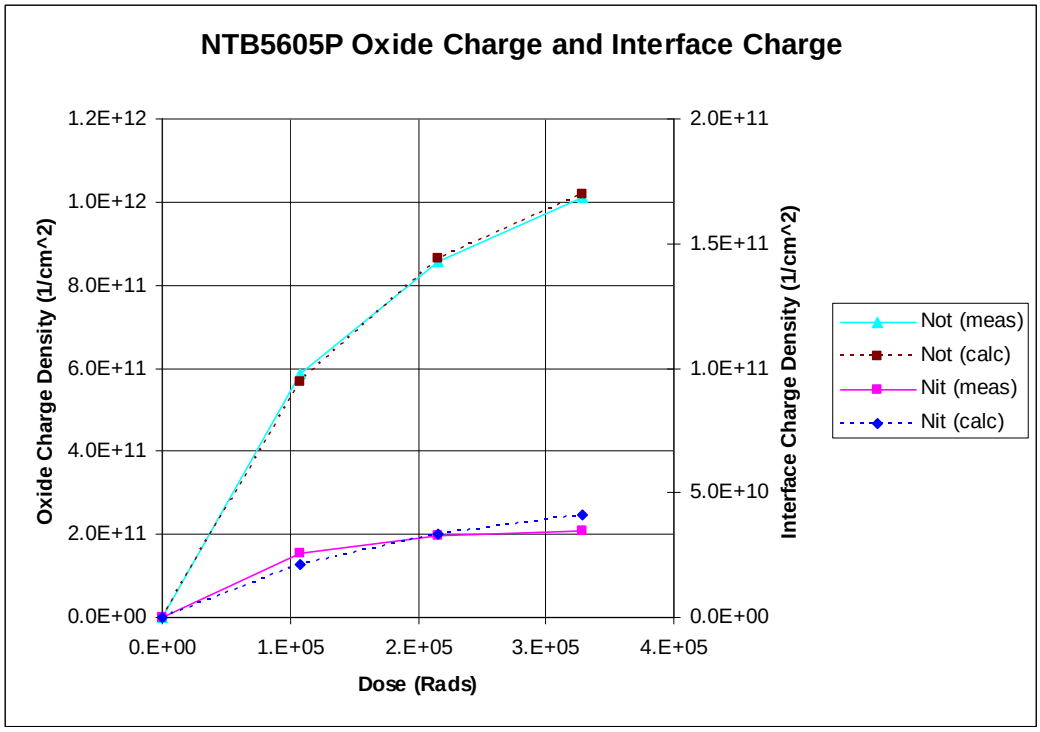

Figure 14 Measured and Calculated Values of Oxide-Trapped Charge and Interface-Trapped Charge for the NTB5605P.

11. Measured Total Dose Effects in SOI

In references [29] - [32], measurements of total dose effects in SOI MOSFETs are described. Threshold voltage shifts in the front and back channels were obtained as a function of total dose up to 10 Mrads. Enhanced degradation of the top gate threshold voltage in fully-depleted n-channel devices, such as shown in Fig. 15, was observed in reference [29]. This increased threshold shift in the top channel is due to the coupling to the top gate of the large radiation-induced oxide charge in the buried oxide when the silicon layer is fully depleted.

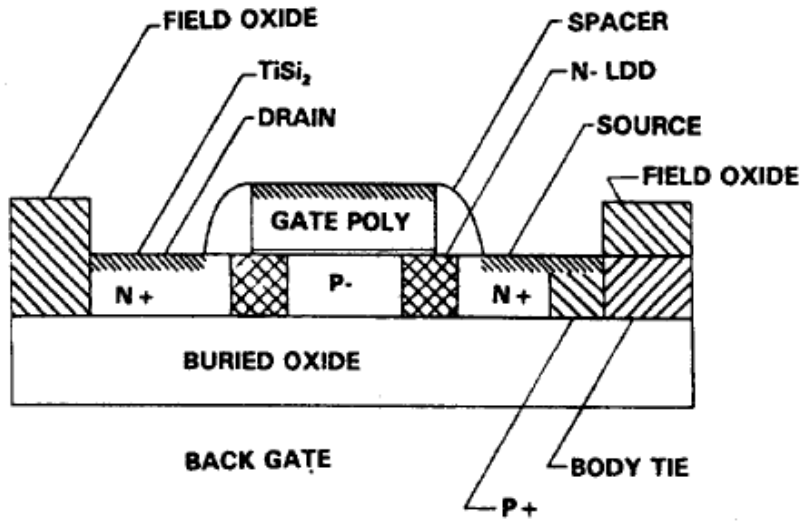

Figure 15 Structure of the Fully-Depleted N-Channel SOI MOSFET.

Charge trapped in the buried oxide will induce a threshold voltage shift in the bottom or back channel according to Equation (1). When the silicon is fully depleted, the charge in the buried oxide will also be coupled to the top gate. If the threshold shift in the bottom channel is ΔV_{bc}, the charge coupled to the top gate will be,

$$Q = C\Delta V_{bc} = \frac{C_{Si}C_{box}}{C_{Si}+C_{box}}\Delta V_{bc}.$$

The effect of Q on the top gate threshold voltage will be,

$$\Delta V_{t1} = -\frac{Q}{C_{tox}} = k_1 \Delta V_{bc}, \qquad (32)$$

where

$$k_1 = \left[\frac{C_{Si} C_{box}}{C_{Si} + C_{box}} \right] \frac{1}{C_{tox}}. \tag{33}$$

As shown in reference [29] there will also be a coupling of the charge trapped in the top gate oxide to the bottom channel described by k_2. Since in these devices the thickness of the buried oxide is much greater than the thickness of the top gate oxide, $k_2 << k_1$, and k_2 can be ignored.

The n-channel device studied in reference [29] had a top gate oxide thickness of $t_{ox} = 15$ nm, a silicon thickness of $t_{Si} = 95$ nm and a buried oxide thickness of $t_{box} = 330$ nm. These dimensions give a value for the coupling parameter $k_1 = 0.0415$. The measured top gate threshold shift as a function of total dose is shown in Fig. 16, and the measured bottom gate shift is shown in Fig. 17. The effect of the buried oxide charge on the top gate threshold voltage is given by Equation (32) and shown in Fig. 16 as DeltaVbg. The trapped charge in the top gate oxide and its associated voltage shift can be calculated using Equation (8). The bias during irradiation was 5.5 volts which gives $E \approx 3.7$ and $Y \approx 0.7$. If we assume a capture cross section of $\sigma_0 = 6 \times 10^{-14}$ and a density of trapping centers, $N_T^{'} = 1.76 \times 10^{12}$, Equation (8) together with Equation (1) gives the shift due to the gate oxide charge shown in Fig. 16 as DeltaVfg. The sum of voltage shifts due to the top and bottom oxide trapped charge agree closely with measured values.

Matching the measured shift in the bottom gate threshold voltage is a little more complicated. The measured values cannot be reproduced by Equation (8) with any reasonable set of parameters. The shape of the curve does not show the expected saturation at large total dose as is seen in Figure 15 of reference [31] or Figure 9 of reference [32] for example.

The measured back channel voltage shift shown in Fig. 17 can be explained if we assume there are two different trapping centers in the buried oxide with different capture cross sections. The primary trap sites have a cross section similar to that seen in the other work reported here, $\sigma_0 = 3 \times 10^{-14} cm^2$, and the second type of trap has a much smaller cross section, $\sigma_0 = 2 \times 10^{-15} cm^2$. Two hole traps with cross sections of this general size were observed in Reference [13]. The traps with smaller cross section may have been present in the studies reported above, but since these studies were for much lower total dose values, the effect of traps with smaller cross section may not have been apparent.

If we assume a density of trapping sites for the larger cross section of $N_T^{'} = 4.0 \times 10^{11}$ and a density of $N_T^{'} = 3.0 \times 10^{11}$ for the smaller cross section, Equation (8) together with Equation (1) yields the curves shown in Fig. 17, where DeltaV1 is the shift from the primary trap sites and DeltaV2 from the secondary trap sites. The sum of the two effects

is very close to the measured threshold shift in the back channel. No interface-trapped charge was observed in these tests.

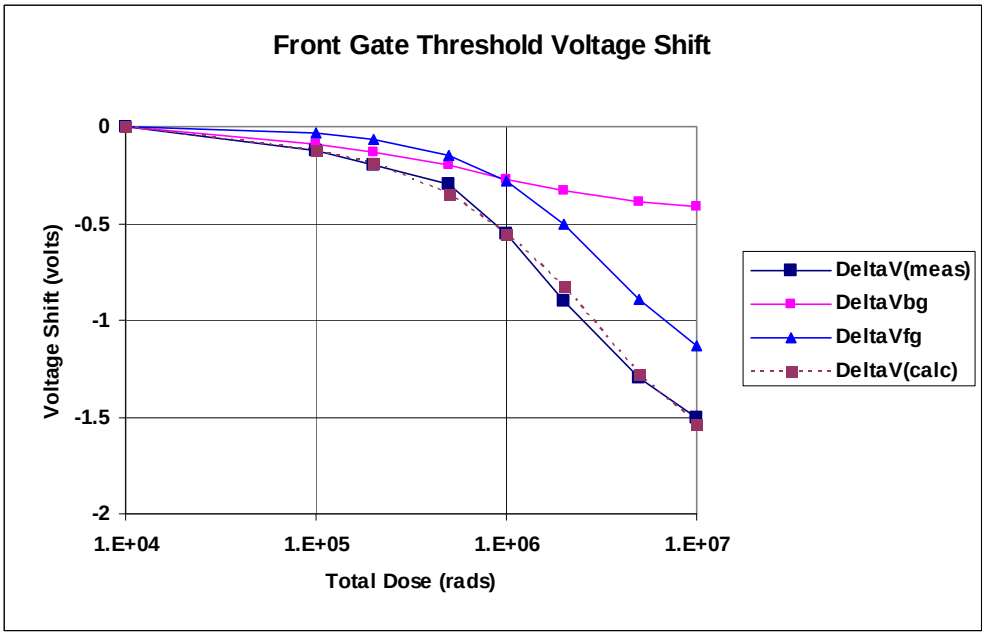

Figure 16 Radiation-Induced Top Gate Threshold Voltage Shift.

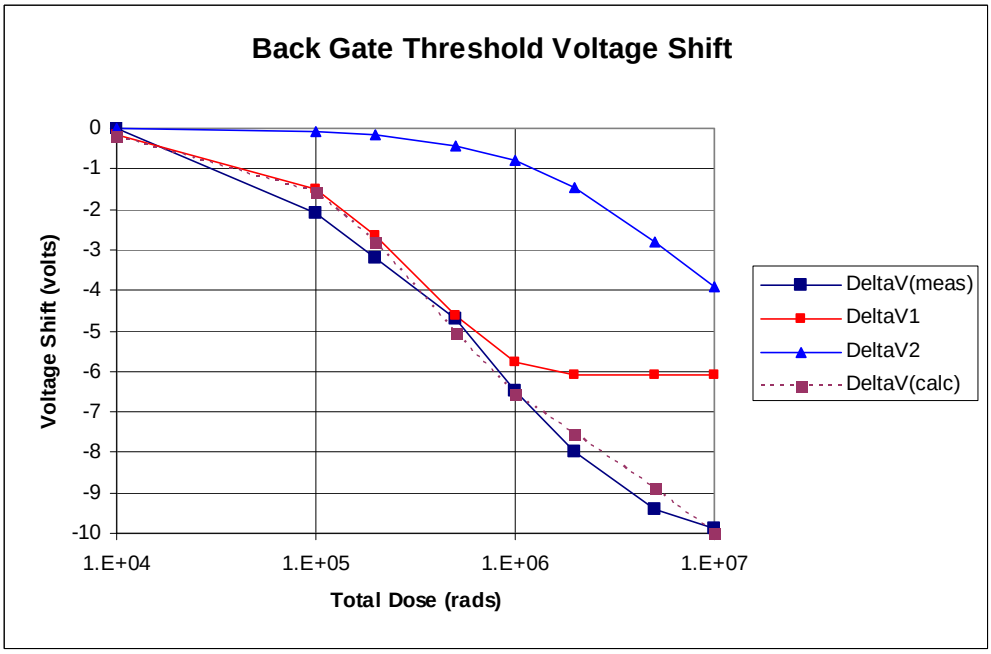

Figure 17 Radiation-Induced Back Gate Threshold Voltage Shift

12. Total Dose Measurements in Bipolar Base Oxides

Although the zero-bias case is especially important for aging calculations (devices in storage with power off), we have so far only analyzed one set of measurements, that for the IRF620. However, in reference [34] zero-bias measurements are available for bipolar-base oxides. Although there are some important differences between these oxides and gate oxides in MOSFETs, the results in reference [34] provide an additional test of the zero-bias model developed for the IRF620.

Interface-trapped charge and oxide-trapped charge for a 600 nm MOS capacitor made with the RF25 process and irradiated at 320 rad/sec. are shown in Fig. 18. This is the low dose-rate case where high dose-rate effects from trapped electrons that were observed in this study do not appear.

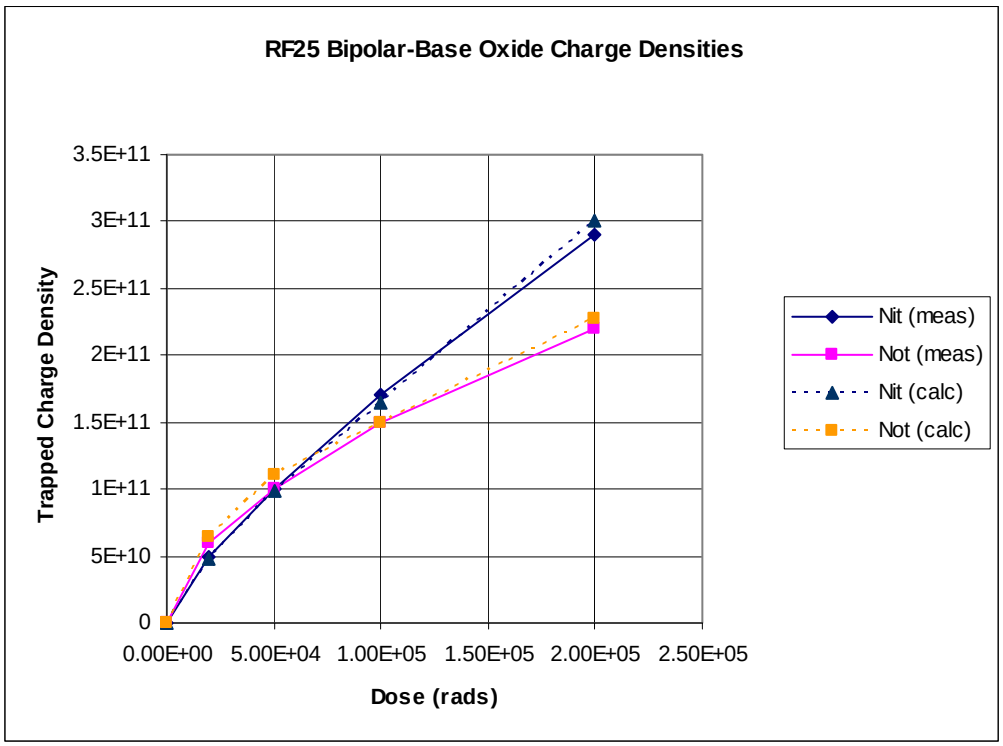

Figure 18. Trapped Charge in Bipolar-Base Oxides Irradiated at Zero Bias.

Neither the bulk model represented by Equations (8) and (16) nor the zero-field model of Equations (30) and (31) match the data in Figure 18 very well. However, in these oxides, t_{ox} = 600 nm, which is 5 times larger than the oxide thickness used in the IRF620 analysis. So the small amount of charge generated in the bulk of the oxide under the small field of the work function difference, ϕ_{ms} = –0.7 V, may contribute significantly in this larger volume of oxide. We find that the data in Figure 18 can be matched with a

combination of the bulk and zero-field models. Some of the trapped charge originates in the bulk of the oxide and the rest is formed directly in the boundary regions of width δ given by Equation (29).

In the combined model we have for the oxide-trapped charge,

$$\begin{aligned}\Delta N_{ot}^{bulk} &= N_T^{'}[1-\exp(-G_0 DY\sigma_T t_{ox})] \\ &= N_T^{'}[1-\exp(-3.67\times10^{-6} D)],\end{aligned}$$

$$\begin{aligned}\Delta N_{ot}^{zf} &= N_T^{'}[1-\exp(-G_0 40\sigma_0 \delta D)] \\ &= N_T^{'}[1-\exp(-19.4\delta D)],\end{aligned}$$

and for the interface-trapped charge,

$$\begin{aligned}\Delta N_{it}^{bulk} &= N_D^{'}[1-\exp(-G_0 DY\sigma_H t_{ox})] \\ &= N_D^{'}[1-\exp(-0.29\times10^{-6} D)],\end{aligned}$$

$$\begin{aligned}\Delta N_{it}^{zf} &= N_D^{'}[1-\exp(-G_{0H}\sigma_H \delta D)] \\ &= N_D^{'}[1-\exp(-0.486\delta D)].\end{aligned}$$

In these equations, $E = 0.01$, Y=0.01 with $\sigma_T = \sigma_0 E^{-0.55}$ and $\sigma_0 = 6\times10^{-14}$ together with $\sigma_H = 6\times10^{-14}$. The density of trapping sites is $N_T^{'} = 2.35\times10^{11}$ and the density of hydrogen-containing defects is $N_T^{'} = 4.2\times10^{12}$. The total trapped charge densities are $\Delta N_{ot} = \Delta N_{ot}^{bulk} + \Delta N_{ot}^{zf}$ and $\Delta N_{it} = \Delta N_{it}^{bulk} + \Delta N_{it}^{zf}$ which are plotted in Fig. 18 in good agreement with the measurements.

13. Summary of Derived Model Parameters

A summary is given in Table 2 of the bulk model parameters derived in Sections 9 through 12. The table shows the range of variation we see in the basic parameters related to hole trapping, σ_0 and $N_T^{'}$, and H^+ formation, σ_H and $N_D^{'}$. Included in Table 2 are all the tests discussed above except for the specially-hardened oxides studied in reference [14] and the zero-field case for the IRF620.

Table 2. Model Parameters and Trapped Charge for Analyzed Test Cases

Device	E	σ_0	$(1-f_e)N_T^{'}$	σ_H	$N_D^{'}$	Dose	ΔN_{ot}	ΔN_{it}
IRF620	0.80	6×10^{-14}	8.0×10^{12}	3×10^{-14}	6.9×10^{11}	1×10^{5}	1.1×10^{12}	4.4×10^{10}
						2×10^{5}	2.8×10^{12}	1.3×10^{11}
						8×10^{5}	7.5×10^{12}	4.6×10^{11}
MTB30P06	1.4	6×10^{-14}	2.3×10^{13}	1.2×10^{-13}	1.7×10^{11}	1×10^{5}	3.3×10^{12}	7.9×10^{10}
						2×10^{5}	6.5×10^{12}	1.1×10^{11}
						5×10^{5}	1.3×10^{13}	1.3×10^{11}
NTB5605P	1.0	1×10^{-13}	1.2×10^{12}	1.2×10^{-13}	5.0×10^{10}	1×10^{5}	5.9×10^{11}	2.5×10^{10}
						2×10^{5}	8.6×10^{11}	3.3×10^{10}
						3×10^{5}	1.0×10^{12}	3.5×10^{10}
FWS [21]	1.0	1×10^{-13}	1.4×10^{12}	6×10^{-14}	1.6×10^{12}	1×10^{5}	4.3×10^{11}	2.5×10^{11}
						2×10^{5}	4.0×10^{11}	2.7×10^{11}
						5×10^{5}	7.8×10^{11}	5.7×10^{11}
Test I [14]	2.0	3×10^{-14}	1.6×10^{12}	6×10^{-14}	1.0×10^{11}	2×10^{4}	1.2×10^{11}	2.2×10^{10}
TopG [29]	3.7	6×10^{-14}	1.7×10^{12}	0	0	1×10^{5}	0.4×10^{11}	0
SOI						1×10^{6}	4.0×10^{11}	0
						1×10^{7}	1.6×10^{12}	0
BotG [29]	0.2	3×10^{-14}	4.0×10^{12}	0	0	1×10^{5}	1.4×10^{11}	0
SOI		2×10^{-15}	3.0×10^{11}			1×10^{6}	4.2×10^{11}	0
						1×10^{7}	6.5×10^{11}	0
RF25 [34]	0.01	6×10^{-14}	2.3×10^{11}	6×10^{-14}	4.2×10^{12}	2×10^{4}	6.0×10^{10}	5.0×10^{10}
						2×10^{5}	2.2×10^{11}	2.9×10^{11}

The key points revealed in the table are: (1) The hole trapping cross sections are generally in the range of $\sigma_0 = 6\times10^{-14}$ to $\sigma_0 = 12\times10^{-14}$, as measured in reference [12], with one test at the lower end measured in reference [13], $2\times10^{-15} cm^2$. (2) The cross section for H^+ formation σ_H is in the same range as σ_0, and (3) the densities of hole trapping centers and hydrogen-containing defect sites vary considerably depending on oxide processing but are typically in the range of $10^{11} - 10^{12} cm^{-2}$.

14. Space Charge Effects of Trapped Holes

From Table 2 we see that oxide-trapped charge densities greater than $2\times10^{12} cm^{-2}$ are observed in several devices. This immediately suggests that charge of this magnitude trapped near the Si/SiO_2 interface can create a reverse field in the oxide greater than that of the gate bias,

$$E_{rev} = -\frac{q}{\varepsilon_{ox}}\Delta N_{ot} \cong -1 \text{ Mv/cm.}$$

If space charge effects of this magnitude exist, one would never see trapped charge densities higher than the field reversal point for a given gate bias. This is contrary to observation in many cases, including the IRF620 and the MTB30P06V in Table 2.

However, as pointed out in reference [34] oxide-trapped charge near the Si interface is screened by image charge in the Si inversion layer which is equivalent to a dipole sheet as seen from the bulk of the oxide. This situation is a classical problem in electrostatics where the field of a charge situated in a dielectric outside a conducting boundary is represented by the charge plus an image charge an equal distance behind the boundary.

Of course these charge layers are not infinite in extent so the trapped charge and its image do not cancel exactly, but it is possible to estimate the size of the dipole field in the bulk of the oxide. The potential of a dipole sheet where D is the dipole moment is

$$\phi = \int D d\Omega .$$

In the present case the dipole moment is $D = q\Delta N_{ot}\delta$ where δ is a few nanometers, comparable to the width of the region of oxide-trapped charge near the interface. If for convenience we assume the interface is a circular area of radius R, the element of solid angle seen from a position x in the bulk of the oxide is

$$d\Omega = 2\pi \frac{rdr}{\left(r^2 + x^2\right)} \frac{x}{\sqrt{r^2 + x^2}} .$$

The size of the charge sheet, R, is on the order of the channel length or width in a MOSFET, and the integral over solid angle becomes

$$\phi = 2\pi\left[1 - \frac{x}{\sqrt{R^2 + x^2}}\right]D.$$

Note that as $R \to \infty$, $\phi \to 2\pi D$, and the field is $E_{rev} = -\frac{d\phi}{dx} = 0$. Otherwise the magnitude of the field in the oxide at a distance x from an interface of lateral size R is,

$$E_{rev} \cong \frac{D}{\varepsilon_{ox}}\frac{2\pi}{R}\left(1 - \frac{x}{R^2}\right) = 2\pi\frac{q}{\varepsilon_{ox}}\Delta N_{ot}\frac{\delta}{R}\left(1 - \frac{x^2}{R^2}\right),$$

where an approximation for $x << R$ has been made.

Since $\delta \approx 1$ nm (10^{-9} m) and $R \approx 1$ micron (10^{-6} m), the reverse field due to trapped charge near the interface is screened effectively for the usual situation in MOSFETs.

14. Use of the Total Dose Model in Circuit Simulation

By far the best approach to including MOSFETs with total dose effects in circuit simulation is to use measured I-V curves to obtain VTO and U0 by parameter extraction as a function of radiation dose for a particular device. The code can then interpolate between the measured values to obtain parameters at intermediate values of dose.

Another preferred method is to measure directly ΔN_{ox} and ΔN_{it} in a particular device exposed to radiation using either charge-pumping, midgap or other measurement techniques [33] together with Equations (1) - (4) which are implemented in the simulator models. Equations (1) – (4) are easily incorporated in any SPICE MOSFET model with the necessary parameters provided as input. In Fig.19 are shown measured and calculated I-V curves at 200 Krad for the MTB30P06V. The calculated curves were obtained with SPICE-based simulation using input values for interface and oxide-trapped charge shown in Fig. 12.

If direct measurements of device performance are not available, then the analytical model, Equations. (8) and (16), can be used to calculate ΔN_{ox} and ΔN_{it} from which threshold voltage and mobility are obtained from Eqns. (1) - (4). This approach is, of course, more uncertain than using directly measured values because the model requires a number of parameters that have to be inferred from other measurement and analysis. A useful guide to typical values of the necessary parameters is given in Table 2.

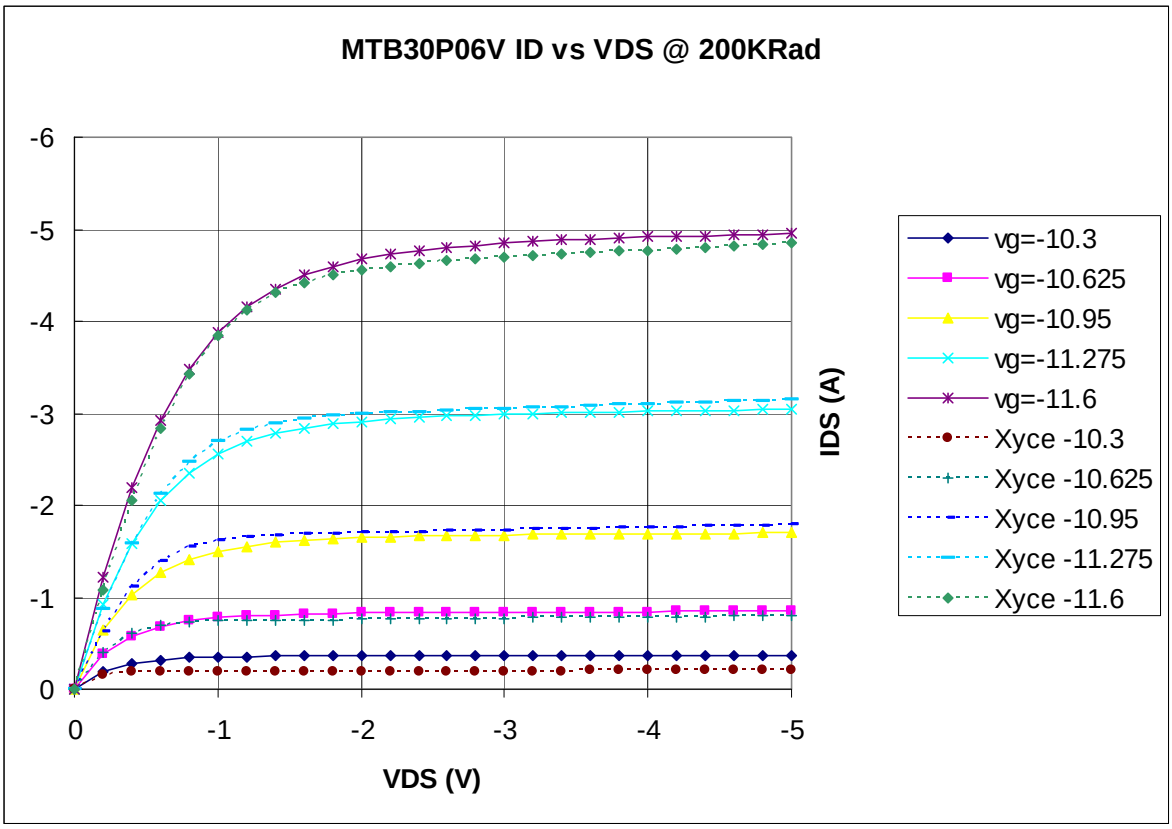

Figure 19 Measured and Calculated Drain Curves for the MTB30P06V at 200 Krad.

15. Long Term Effects – Aging

To look at aging (the effects of very low dose rates over long periods of time), we need to combine the buildup of oxide-trapped charge given by the time-dependent solution of Equation (6) and recombination by thermal emission and electron tunneling, Equation (27). Under the conditions discussed above relating to Figure 2, the combined effects for positive gate bias are represented by,

$$\Delta V_{ot} = -\frac{q}{\varepsilon_{ox}} \bar{x} N_T' \left[1-\exp\left(-G_0 \sigma_T Y t_{ox} R t\right)\right] \int_{\phi_m(t)}^{\phi_c} p_2(\phi_t) d\phi_t \left[\left(1-\frac{x_m}{x_0}\right)-\frac{x_0}{2t_{ox}}\left(1-\frac{x_m^2}{x_0^2}\right)\right], \quad (34)$$

where $\bar{x} = t_{ox}$. In Equation (34), the first term in brackets is the buildup of trapped charge ahead of the electron tunneling front, the integral term is the recombination by thermal emission and the last term in brackets is recombination by electron tunneling. For negative gate bias during irradiation, trapping will be near the gate and we can adopt the value $\bar{x} = 0.2 t_{ox}$, but since the charge distribution is assumed to be broad, electron tunneling will probably be negligible.

Since interface-trapped charge does not recombine at room temperature, the buildup is described by the time-dependent solution equivalent to Equation (16),

$$\Delta V_{it} = dtype \frac{q}{C_{ox}} N_D' \left[1-\exp\left(-G_0 \sigma_H Y t_{ox} R t\right)\right], \quad (35)$$

where dtype=1 for NMOS with positive bias. The steady buildup of interface-trapped charge under positive gate bias will also reduce the mobility according to Equation (4).

For PMOS with negative bias, the H^+ generated cannot reach the silicon interface until the bias is removed, and even then the hydrogen ions may have been partly eliminated at the gate. H^+ ions that reach the gate will pick up an electron to produce H_0 which is highly reactive and may dimerize to produce H_2. The longer a negative bias is on, the smaller the eventual formation of interface trapped charge. Switched-gate bias experiments demonstrating these effects are reported in reference [35]. The worst case total dose situation for PMOS occurs with zero gate bias.

We turn our attention now to the aging of a MOS device that is powered off, i.e. the oxide field is approximately zero during a long period of irradiation at low dose rate. In this situation the net buildup of holes in the oxide will be the result of electron diffusion out through the boundaries as discussed in the analysis for the IRF620. At low dose rate Equation (29) will not apply, however, since $\delta \to t_{ox}$, and one must resort to a full calculation of the accumulated charge in the oxide under the competing effects of generation, recombination and diffusion. The macroscopic processes are described by

the ambipolar diffusion equation [36], although calculation of the initial electron-hole recombination lifetime requires more detailed considerations [37].

To develop a solution to the problem of charge generation at low dose rate under zero field conditions, first consider the calculation of the yield curve in Fig. 1 which was obtained experimentally [6]. This curve was derived essentially by counting the number of electrons that leave a 105 nm oxide after irradiation under different values of oxide field. The uncompensated holes remain in the oxide and can be measured.

It should be possible to reproduce Fig. 1 with a solution of the ambipolar diffusion equation in the presence of an electric field E [38],

$$D_n \frac{d^2 \delta n}{dx^2} + \mu_n E \frac{\partial \delta n}{\partial x} + G_0 R - \frac{\delta n}{\tau_n} = 0, \tag{36}$$

where δn is the density of radiation-generated free electrons, D_n is the diffusion constant, μ_n is mobility and τ_n is the recombination lifetime.

From the solution of Equation (36) with the boundary condition for an ohmic contact, $\delta n = 0$ at x=0, the electron flux per unit area out of the oxide at the gate is,

$$J_n = -D_n \left. \frac{d\delta n}{dx} \right|_{x=0}$$

$$= -G_0 R L_n \sqrt{1+\beta^2} \left[\frac{\cosh\left(\frac{t_{ox}}{L_n} \sqrt{1+\beta^2} \right) - e^{\beta t_{ox}/L_n}}{\sinh\left(\frac{t_{ox}}{L_n} \sqrt{1+\beta^2} \right)} + \frac{\beta}{\sqrt{1+\beta^2}} \right], \tag{37}$$

where $\beta = \frac{EL_n}{2(kT/q)}$. In Equation (37) $L_n = \sqrt{D_n \tau_n}$ is the diffusion length or the distance an electron travels on average before recombining. Since $G_0 R t_{ox}$ is the corresponding rate electrons are generated by radiation, the yield measured by this method will be,

$$Y = \frac{L_n}{t_{ox}} \sqrt{1+\beta^2} \left[\frac{\cosh\left(\frac{t_{ox}}{L_n} \sqrt{1+\beta^2} \right) - e^{\beta t_{ox}/L_n}}{\sinh\left(\frac{t_{ox}}{L_n} \sqrt{1+\beta^2} \right)} + \frac{\beta}{\sqrt{1+\beta^2}} \right]. \tag{38}$$

Note that in Equation (38) as $E \to 0$,

$$Y \to \frac{L_n}{t_{ox}} \tanh\left(\frac{t_{ox}}{2L_n}\right), \tag{39}$$

and as $E \to \infty$ $Y \to 1$ as expected. In taking the limit where $E \to \infty$, one must first substitute in the exponentials, $\sqrt{1+\beta^2} = \beta\sqrt{1+1/\beta^2} \cong \beta\left(1+\frac{1}{2\beta^2}+...\right)$.

One finds that if $t_{ox} / L_n = 24$, Y given by Equation (38) falls right on top of the measured points in Figure 1. The only exception is for E=0.01 where the calculated value of Y= 0.04 is a bit high. However, this is in an area where the assumption underlying Fig. 1, that $\sigma_T = \sigma_0 E^{-0.55}$, may be a little suspect. With zero oxide field one would expect Y to be small but not strictly zero, because the electrons within a diffusion length of the boundary will be lost leaving uncompensated holes. The diffusion length L_n in this analysis plays the same role as δ did for the high-dose-rate case considered for the IRF620. These parameters have comparable values, with L_n = 4.38 nm from the analysis of Fig. 1, and δ = 2.19 nm in the analysis of the IRF620.

One must now ask, is the value derived from the measurements in Fig. 1, $t_{ox} / L_n = 24$, reasonable on theoretical grounds. From reference [37] we find the mobility of electrons in SiO_2 is typically 20 cm^2 / V sec, and the recombination lifetime is less than a picosecond. Using an electron mobility of 20, the value of $L_n = t_{ox} / 24$ implies a lifetime of $\tau = 3.8\times10^{-13}$ sec. which is in the expected range. These numbers derived from Fig. 1 together with an oxide thickness of 70 nm give $t_{ox} / L_n = 16.8$. This value substituted in Equation (38) gives a nearly perfect match to the yield curve shown in Fig. 3.5 of reference [37] (dating from 1976).

With a value of Y=0.04 derived from Equation (39), the low-dose buildup of trapped charge in the oxide ahead of the tunneling front will be given by Equation (8). Or alternatively since $Y = L_n / t_{ox}$, Equation (8) reduces to Equation (30) with δ replaced by L_n, as one would expect from the physics. All the considerations discussed in the analysis of the IRF620 with zero oxide field will apply here. The uncompensated holes are created near the silicon interface in the region of the trapping sites and will instantly be trapped. Hydrogen is released in this region near the interface trap sites. Assuming $x_0 << t_{ox}$ the net effect of aging at zero gate bias is then,

$$\Delta V_{ot} = -\frac{q}{\varepsilon_{ox}} \bar{x} N_T' \left[1-\exp\left(-G_0 \sigma_T L_n R t\right)\right] \int_{\phi_m(t)}^{\phi_s} p_2(\phi_t) d\phi_t \left[1-\frac{1}{\beta x_0}\ln(\alpha t)\right], \tag{40}$$

where $\bar{x} = t_{ox}$, $\sigma_T \approx 40\sigma_0$, $L_n = \sqrt{D_n \tau_n}$ and $D_n = (kT/q)\mu_n$. The buildup of interface-trapped charge is given by

$$\Delta V_{it} = dtype \frac{q}{C_{ox}} N_D^{'} \left[1 - \exp\left(-G_0 \sigma_H L_n R t\right)\right] . \tag{41}$$

17. Test of Combined Effects in Aging.

In reference [39] experiments were done to investigate the "rebound" effect in which the threshold shift in n-channel devices due to radiation exposure rebounds as the (negative) oxide charge anneals while the (positive) interface charge does not. Figure 20 illustrates the measurements of voltage shifts from oxide and interface charge during one hour of radiation at a dose rate of 1 Mrad/hour and subsequent anneal at 300 deg. K and 400 deg. K. At the higher temperature all of the oxide-trapped charge is neutralized after 1000 hours. The interface-trapped charge shows little if any annealing even at 125 deg. C.

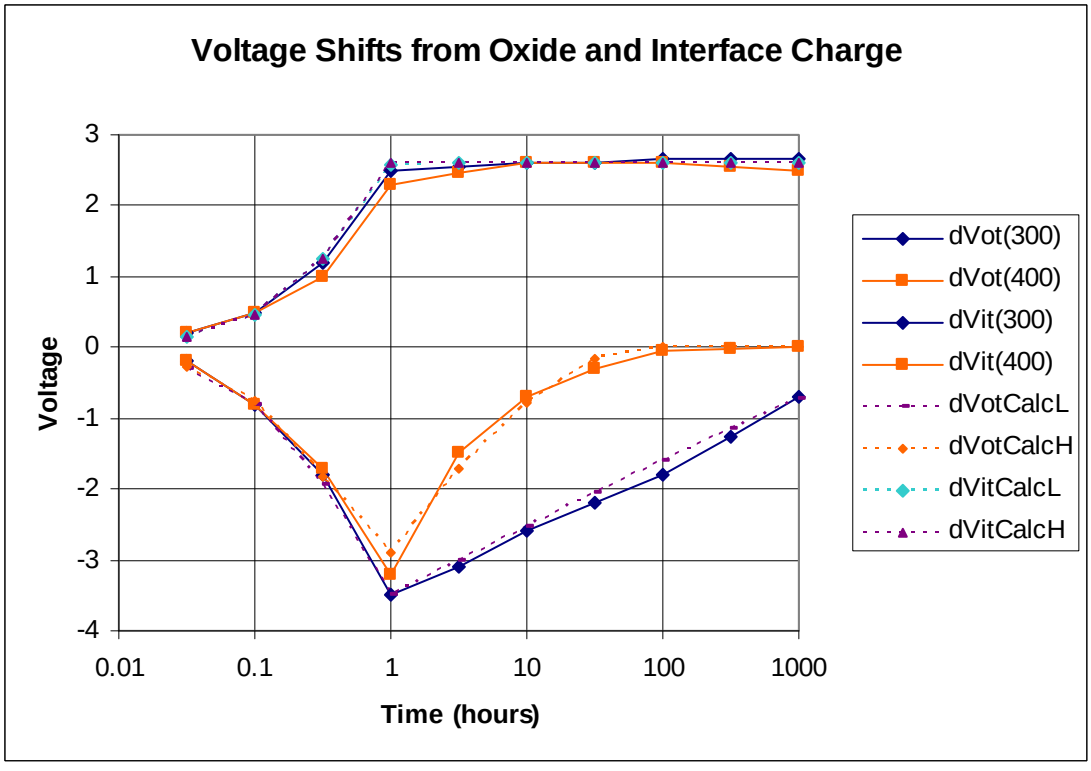

Figure 20. Voltage Shifts from Trapped Charge during Irradiation and Annealing.

The devices used in these experiments were constructed with Sandia's 4/3 micron technology with an oxide thickness of 45 nm. It should be possible to reproduce the measurements in Fig. 20 with the combined-effects model, Equations (34) and (35). The devices were irradiated with $R = 1\times10^{6}$ rad/hour for one hour under a 10 V bias. Thus, $E = 2.22$ MV/cm, $E^{-0.55} = 0.648$ and Y=0.65. If we take for the cross sections, $\sigma_T = \sigma_0 E^{-0.55}$ with $\sigma_0 = 1.9\times10^{-13}$ and $\sigma_H = 6\times10^{-14}$ along with a density of oxide trap sites, $N_T^{'} = 2.71\times10^{12}$, and hydrogen-containing defects, $N_D^{'} = 1.64\times10^{12}$, the model reproduces the radiation curves up to 1 hour as shown by the dashed curves in Fig. 20.

During the annealing phase we must choose $\alpha = 8.44$ and $\beta x_0 = 11.05$ for the electron tunneling parameters, and $A = 3\times10^{5}$ for the thermal annealing constant, where time is counted in hours. The thermal annealing shown in Fig.20 requires the energy distribution of oxide trapped holes given in Fig. 21. This twin-peak distribution is similar to that of Fig. 2 and other cases reported in reference [22]. The twin-peak energy distribution is suggestive of two distinct trapping centers which may have different cross sections as reported in reference [13] and discussed above in Section 11. The value for βx_0 required to match Fig. 20 implies the width of the region of trapped charge is $x_0 = 1.7$ nm, similar to that derived from Fig. 10 for the IRF130.

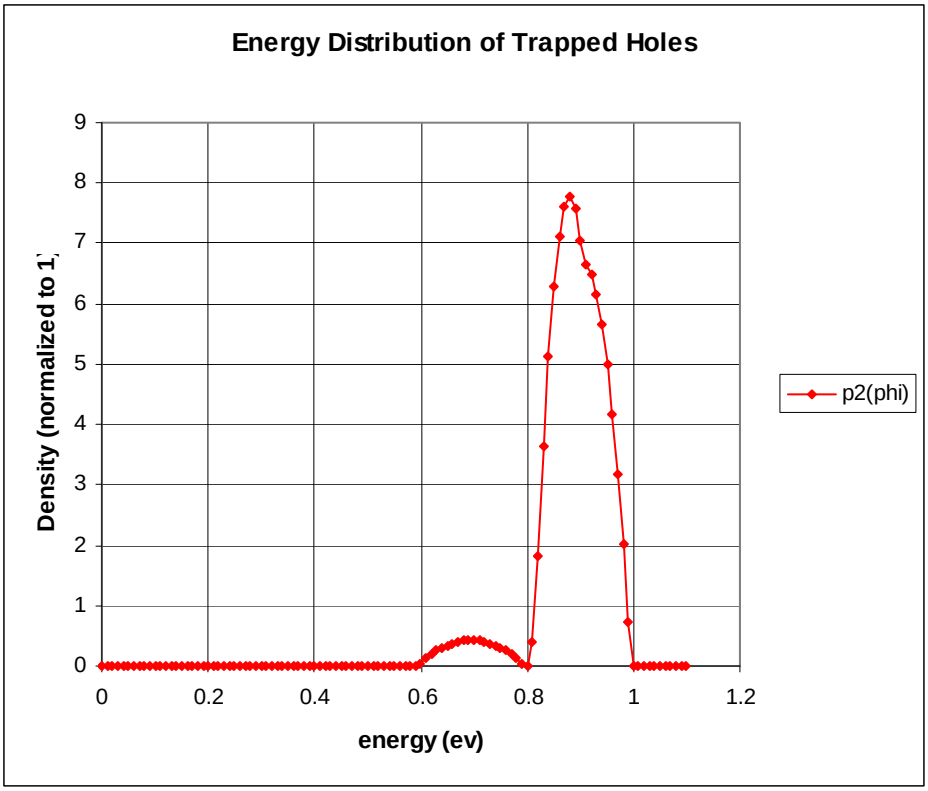

Figure 21. Energy Distribution of Trapped Holes Implicit in Figure 20

17. Summary and Conclusions

Relatively simple formulas for the density of oxide-trapped charge and interface-trapped charge as a function of total dose have been derived. These formulas are able to match a large number of measurements, the parameters of which are summarized in Table 2. The matches for oxide charge require values of capture cross sections for holes and the density of trapping sites. For interface charge one needs the density of hydrogen-containing defects in the oxide and the cross section for H^+ formation by holes. The cross sections have been measured and are verified within reasonable limits by the results in Table 2. Densities of hydrogen-containing defects and oxide traps vary due to processing, but the range of observed values is reasonably well defined in Table 2. Special hardened oxides may have much smaller values as shown in Table 1.

The basic formulas for the effects of trapped charge, Equations (1) – (4), are easily incorporated into SPICE-like compact models. The calculation of oxide-trapped charge and interface-trapped charge for MOSFETs irradiated under bias follows from Equations (8) and (16) which describe charge produced in the bulk of the oxide. For irradiation under zero bias, charge is produced in regions near the boundaries where electrons can escape by diffusion. The zero-field model is described by Equations (29), (30), and (31).

Expressions for aging of MOSFETs by low dose radiation exposure over long time periods with positive gate bias are given in Equations (34) and (35). With negative gate bias, the centroid of the charge distribution is smaller but electron tunneling is negligible. Interface charge buildup may be negligible over long time periods with negative bias, because the H^+ will be removed at the gate. The aging by low dose rate radiation with zero gate bias is given by Equations (40) and (41). In devices with thick gate oxides, analysis of zero-field irradiation effects may require a combination of the bulk and zero-field models. In oxides with narrow regions of oxide trapped charge, $x_0 \approx 1.7$ nm, the electron tunneling front can remove all of the oxide-trapped charge in a few years.

The main objective of this work is to obtain analytical expressions for total dose effects simple enough to include in SPICE-like simulation codes. As a result, a number of effects have been glossed over; primarily transport effects such as the time for buildup of interface-trapped charge and the space charge effects possibly leading to reduced interface trap formation at high dose rates [34]. Transport effects involve field calculations, charge distributions and such issues as polaron hopping which are more appropriate for numerical models.

References

1. J. R. Schwank, "Total Dose Effects in MOS Devices", IEEE Nuclear and Space Radiation Effects Conference Short Course (2002).

2. J. R. Schwank, F. W. Sexton, P. E. Dodd and M. R. Shaneyfelt, "Radiation Effects", Sandia National Laboratories Report SAND2003-1872P (2003).

3. Yuan Taur and Tak H. Ning, *Fundamentals of Modern VLSI Devices*, Cambridge University Press, New York, 1998, Section 2.3.7.1.

4. F. W. Sexton and J. R. Schwank, "Correlation of Radiation Effects in Transistors and Integrated Circuits", IEEE Trans. Nucl. Sci. Vol. 32, No. 6, pp. 3975-3981 (1985).

5. D. Zupac, K. F. Galloway, P. Khosropour, S. R. Anderson, and R. D. Schrimpf, "Separation of Effects of Oxide-Trapped Charge and Interface-Trapped Charge on Mobility in Irradiated Power Mosfets", IEEE Trans. Nucl. Sci., Vol. 40 , 1307 (1993).

6. M. R. Shaneyfelt, D. M. Fleetwood, J. R. Schwank, and K. L. Hughes, "Charge Yield for Cobalt-60 and 10 Kev X-Ray Irradiations", IEEE Trans. Nucl. Sci., Vol. 38, No. 6, 1187-1194 (1991).

7. H. E. Boesch, Jr., J. M. McGarrity and F. B. McLean, "Temperature- and Field-Dependent Charge Relaxation in SiO_2 Gate Insulators", IEEE Trans. Nucl. Sci., Vol. 25, No. 3, pp. 1012-1016 (1978).

8. H. E. Boesch, Jr., F. B. McLean, J. M. McGarrity and P. S. Winokur, "Enhanced Flatband Voltage Recovery in Hardened Thin MOS Capacitors", IEEE Trans. Nucl. Sci., Vol. 25, No. 6, pp. 1239-1245 (1978).

9. F. B. McLean, G. A. Ausman, Jr., H. E. Boesch, Jr. and J. M. McGarrity, "Application of Stochastic Hopping Transport to Hole Conduction in Amorphous SiO_2", J. Appl. Phys., Vol. 47, pp. 1529-1532 (1976).

10. Tak H. Ning, "Capture Cross Section and Trap Concentration of Holes in Silicon Dioxide", J. Appl. Phys., Vol. 47, 1079 (1976).

11. S. N. Rashkeev, C. R. Cirba, R. D. Schrimpf, A. Michez, and S. T. Pantelides, "Physical Model for Enhanced Interface-Trap Formation at Low Dose Rates", IEEE Trans. Nucl. Sci., Vol. 49, 2650 (2002).

12. J. J. Tzou, J. Yuan-Chen Sun, and Chih-Tang Sah, “Field Dependence of Two Large Hole Capture Cross Sections in Thermal Oxide on Silicon”, Appl. Phys. Lett., Vol. 43, 861 (1983).

13. A. R. Stivers, and C. T. Sah, “A Study of Oxide Traps and Interface States of the Silicon-Slicon Dioxide Interface”, J. Appl. Phys. Vol. 51(12), pp. 6292-6304 (1980).

14. D. M. Fleetwood, S. L. Miller, R. A. Reber, Jr., P. J. McWhorter, P. S. Winokur, M. R. Shaneyfelt, and J. R. Schwank, “ New Insights into Radiation-Induced Oxide_Trap Charge Through Thermally-Stimulated-Current Measurement and Analysis”, IEEE Trans. Nucl. Sci. Vol. 39, No. 6, pp. 2192-2203 (1992).

15. M. R. Shaneyfelt, J. R. Schwank, D. M. Fleetwood, P. S. Winokur, K. L. Hughes, G. L. Hash, and M. P. Connors, “Interface Trap Buildup Rates in Wet and Dry Oxides”, IEEE Trans. Nucl. Sci. Vol. 39, No. 6, pp. 2244-2251 (1992).

16. B. J. Mrstik and R. W. Rendell, “ $Si-SiO_2$ Interface State Generation During X-Ray Irradiation and During Post-Irradiation Exposure to Hydrogen Ambient”, IEEE Trans. Nucl. Sci. Vol. 38, 110 (1991).

17. R. E. Stahlbush, H. H. Edwards, D. L. Griscom and B. J. Mrstik, “Post Irradiation Cracking of H_2 and Formation of Interface States in Irradiated Metal-Oxide-Semiconductor Field-Effect Transistors”, J. Appl. Phys., 73 (2), 658 (1993).

18. S. N. Rashkeev, D. M. Fleetwood, R. D. Schrimpf and S. T. Pantelides, “Defect Generation by Hydrogen at the $Si-SiO_2$ Interface”, Phys. Rev. Lett., Vol. 87, No. 16, p. 165506-1 (2001).

19. S. N. Rashkeev, D. M. Fleetwood, R. D. Schrimpf and S. T. Pantelides, “ Proton-Induced Defect Generation at the $Si-SiO_2$ Interface”, IEEE Trans. Nucl. Sci. Vol. 48, No. 6, pp. 2086-2092 (2001).

20. D. B. Brown and N. S. Saks, “Time Dependence of Radiation-Induced Interface Trap Formation in MOS Devices as a Function of Oxide Thickness and Applied Field”, J. Appl. Phys. Vol. 70 (7), pp. 3734-3747 (1991).

21. D. M. Fleetwood, P. S. Winokur, and J. R. Schwank, “Using Laboratory X-Ray and Cobalt-60 Irradiations to Predict CMOS Device Response in Strategic and Space Environments”, IEEE Trans. Nucl. Sci. Vol. 35, 1497 (1988).

22. P. J. McWhorter, S. L. Miller and W. M. Miller, “Modeling the Anneal of Radiation-Induced Trapped Holes in a Varying Thermal Environment”, IEEE Trans. Nucl. Sci. Vol. 37, No. 6, pp. 1682-1689 (1990).

23. See reference [3], Section 2.4.3.

24. F. P. Heiman and G. Warfield, “The Effects of Oxide Traps on the MOS Capacitance”, IEEE Trans. Electron Devices, ED-12, 167-178, (1965).

25. T. R. Oldham, A. J. Lelis, and F. B. McLean, “Spatial Dependence of Trapped Holes Determined From Tunneling Analysis and Measured Annealing”, IEEE Trans. Nucl. Sci. Vol. 33, 1203-1209 (1986).

26. C. Picard, C. Brisset, O. Quittard, M. Marceau, A. Hoffman, F. Joffre, J-P. Charles, “Use of Commercial VDMOSFETs in Electronic Systems Subjected to Radiation”, IEEE Trans. Nucl. Sci. Vol. 47, 627 (2000).

27. S. M. Sze and K. K. Ng, *Physics of Semiconductor Devices*, Wiley-Interscience, Third Edition, New York, 2007, Chapter 4, Figure 22.

28. Albert Nunez, private communication (2007).

29. W. C. Jenkins and S. T. Liu, “Radiation Response of Fully-Depleted MOS Transistors Fabricated in SIMOX”, IEEE Trans. Nucl. Sci. Vol. 41, No. 6, pp. 2317-2321 (1994).

30. S. T. Liu and W. C. Jenkins, “The Effect of Power Supply Voltage Scaling on the Total Dose Radiation Response of Fully-Depleted SOI MOS Transistors”, IEEE Trans. Nucl. Sci. Vol. 42, No. 6, pp. 2122-2126 (1995).

31. S. T. Liu, W. C. Jenkins and H. L Hughes, “Total Dose Radiation Hard 0.35 micron SOI CMOS Technology”, IEEE Trans. Nucl. Sci. Vol. 45, No. 6, pp. 2442-2449 (1998).

32. S. T. Liu, S. Balster and W. C. Jenkins, “Worst Case Total Dose Radiation Response of 0.35 micron SOI CMOSFETS”, IEEE Trans. Nucl. Sci. Vol. 46, No. 6, pp. 1817-1823 (1999).

33. J. R. Schwank, D. M. Fleetwood, M. R. Shaneyfelt and P. S. Winokur, “A Critical Comparison of Charge-Pumping, Dual-Transistor, and Midgap Measurement Techniques”, IEEE Trans. Nucl. Sci. Vol. 40, No. 6, pp. 1666-1677 (1993).

34. D. M Fleetwood, L. C. Riewe, and J. R. Schwank, “Radiation Effects at Low Electric Fields in Thermal, SIMOX and Bipolar-Base Oxides”, IEEE Trans. Nucl. Sci. Vol. 43, No. 6, pp. 2537-2546 (1996).

35. N. S. Saks, D. B. Brown and R. W. Rendell, “Effects of Switched Gate Bias on Radiation-Induced Interface Trap Formation,” IEEE Trans. Nucl. Sci. Vol. 38, No. 6, pp. 1130-1139 (1991).

36. J. P. McKelvey, *Solid State and Semiconductor Physics*, Harper and Row, 1986

37. T. P Ma and P. V Dressendorfer, Ionizing Radiation Effects in MOS Devices and Circuits, Section 3.2.3, John Wiley and Sons, 1989.

38. T. F. Wunsch and C. L. Axness, “Modeling the Time-Dependent Transient Radiation Response of Semiconductor Junctions”, IEEE Trans. Nucl. Sci. NS-39(6) (1992)

39. J. R. Schwank, P. S. Winokur, P. J. McWhorter, P. W. Sexton, P. V. Dressendorfer, and D. C. Turpin, “Physical Mechanisms Contributing to Device Rebound”, IEEE Trans. Nucl. Sci. NS-31 (6), 1434-1438 (1984)

Appendix

```
/*
 *  File name:  anneal.c
 *   Calculate anealing curves from electron tunneling and thermal emission
 *   Reproduces Fig. 2 in Total Dose Report
 *   gcc -O2 anneal.c -o test1 -lm
 */

#include <stdio.h>
#include <math.h>

#define NREC0    100000
#define NREC1    1100

main(int argc, char *argv[])
{
   int n, i, i0, imax, j, j0;
   double time, scratch[NREC0], p0[NREC0], p1[NREC1];
   double alpha, beta, betax0, deltaVot, T, delta;
   double deltNot, XmX0, e;
   double tox, x0, h, len, Eb, Const= 4.638e-7, A=100;
   int NREC = NREC0;

   tox   = 6e-6;
   alpha = 8.44;
   beta  = 6.5e+7;
   deltNot = 5.2e+11;
   x0 = 3.85e-7;
   h  = tox/(double)NREC;
   betax0 = beta*x0;
   printf(" dNot = %.4e, tox = %.4e, x0 = %.4e, alpha = %.4f, beta = %.4e \n",
deltNot,tox,x0,alpha,beta);

   len  = 0;
   imax = 0;
   for(i=0; i<NREC0; i++)
   {
     scratch[i] = (double)i + 0.5;
     if(len <= x0)
     {
       p0[i] = deltNot/x0;
       imax = i;
     } else
     {
       p0[i] = 0;
```

```
    }
    len += h;
  }
  printf(" imax = %i\n", imax);

  T = 300;
//   T = 400;
  printf(" Temp = %.0f\n", T);

  // distribution of trapped charge in energy
  // Eb is the energy above the valence band in eV.
  // Eb = (double)j/1000;
  double sum=0;
  for(j=0; j<NREC1; j++)
  {
    p1[j] = 0;
  }
  for(j=0; j<NREC1; j++)
  {
    e = (double)j/1000;
    if(j >= 310 && j < 790)
    {
      p1[j] = 0.55-(e-0.55)*(e-0.55)/0.1047;
    }
    if(j >=850 && j < 1250)
    {
      p1[j] += 3.1-(e-1.05)*(e-1.05)/0.012905;
    }
    sum += p1[j]*0.001;
  }
  printf(" sum= %f\n", sum);
  for(j=0; j<NREC1; j++)
  {
    p1[j] /= sum;
  }

  time = 0.1;
  for(n=0; n<9; n++)
  {
    // this section calculates reduction of trapped charge by electron tunneling
    deltaVot = 0;
    i0 = imax*log(alpha*time)/(betax0);
    // analytical expression of trapped charge integral for p0=const
    XmX0 = log(alpha*time)/betax0;
    if(XmX0 > 1) XmX0 = 1;
    deltaVot = -Const*tox*deltNot*((1-XmX0)-0.5*(x0/tox)*(1-XmX0*XmX0));
```

```
    // this section calculates reduction of trapped charge by thermal emission
    delta = 0;
    j0 = (int)(8.616e-5*T*1000*log(A*T*T*time));
    if(j0 < 0) j0 = 0;
    if(j0 > NREC1) j0 = NREC1;
    for(j=j0; j<NREC1; j++)
    {
      delta += p1[j]*0.001;
    }
    printf("   j0 = %i, delta = %f\n", j0,delta);
    deltaVot *= delta;
    printf(" log(time) = %.0f, deltaVot = %.4f, i0 = %i\n", log10(time),deltaVot,i0);

    time *= 10;
   }

}
```

DISTRIBUTION:

1	MS 0157	H. Morgan, 1030
1	MS 0824	M. Prairie, 1510
1	MS 1411	A. Roach, 1814
1	MS 0836	J. Lash, 1516
1	MS 0431	L. J. Lorence, 511
1	MS0429	R. Hartwig. 2100
1	MS 1393	D. R. Weiss, 2110
1	MS 0427	S. Klenke, 2122
1	MS 9003	K. L. Jefferson, 8116
1	MS 9004	W. P. Ballard, 8100
1	MS0316	E. Keiter, 1437
1	MS1071	D. Chu, 1730
1	MS 0525	P. V. Plunkett, 1734
2	MS 0341	C. W. Bogdan, 1734
1	MS 0525	M. F. Deveney, 1734
1	MS 0525	A. Nunez, 1734
1	MS 0525	R. Schells, 1734
1	MS0341	S. D. Wix, 1734
1	MS1072	R. Flores, 1731
1	MS1072	P. Dodd, 1731-1
1	MS 1083	J. R. Schwank, 1731-1
1	MS 1083	M. R. Shaneyfelt, 1731-1
1	MS 0352	C. Hembree, 1731-1
1	MS 0348	G. Laguna, 5353
1	MS 1073	S. Dunlap, 5356
1	MS 9007	B. E. Owens, 8245
2	MS 0807	P. M. Campbell, 9326
1	MS 0807	D. N. Shirley, 9326
1	MS 0899	Technical Library, 9536